Current Pollution Reports (2023) 9:338–358
https://doi.org/10.1007/s40726-023-00253-y

WATER AND SEDIMENT POLLUTION (G TOOR, L NGHIEM AND W ZHANG, SECTION EDITORS)

Removal of Toxic Metals from Water by Nanocomposites through Advanced Remediation Processes and Photocatalytic Oxidation

Ahmad Farhan[1] · Misbah Zulfiqar[1] · Samiah[1] · Ehsan Ullah Rashid[1] · Shahid Nawaz[2] · Hafiz M.N. Iqbal[3] · Teofil Jesionowski[4] · Muhammad Bilal[4] · Jakub Zdarta[4]

Accepted: 20 February 2023 / Published online: 11 April 2023

Abstract

Purpose of Review Heavy and toxic metals are becoming more prevalent in the water sources of the globe, which has detrimental repercussions for both human health and the health of ecosystems. The summary of recent findings on treatment possibilities of toxic metal species by nanomaterials should facilitate the development of more advanced techniques of their removal.

Recent Findings The high concentrations of chromium, mercury, and arsenic identified in wastewater cause a hazard to human health. There is a wide variety of nanoadsorbents and nanophotocatalysts used for heavy/hazardous metal removal. Recent research has resulted in the production of advanced nanostructures that exhibit extraordinary heavy/hazardous metal adsorption effectiveness and photocatalytic diminution of metal ions. These nanostructures have physically and chemically tunable features.

Summary In this review article, the use of carbon-based nanomaterials, polymer-based nanomaterials, and semiconductor-based nanomaterials are extensively discussed to remove mercury, chromium, and arsenic ions from wastewater by the adsorption process. Advanced nanomaterials involved in photocatalytic reduction are also comprehensively discussed.

Keywords Environmental pollutants · Heavy/hazardous metals · Adsorption · Photocatalytic oxidation · Advanced nanocomposites · Wastewater treatment

Introduction

Humans and animals depend on water as the most critical nutrient in their diets. Heavy metals significantly contribute to water contamination, among other factors. Heavy metals are naturally occurring elements with atomic weights greater than water. Hazardous metals may enter the water supply via several natural and human processes, such as the weathering of soils and rocks, volcanic eruptions, and the withdrawal, processing, and exploit of metal contaminants. Copper, arsenic, chromium, lead, cadmium, nickel, and mercury are the heavy or/and hazardous metals that pollute water supplies. Profound metals have the propensity to bioaccumulate in the body, and when consumed more than bio-recommended limits, they cause a wide range of biotoxic consequences [1]. Arsenic (As), mercury (Hg), and chromium (Cr) are the most common metal ions found in polluted water, both from human activities and natural processes.

This article is part of the Topical Collection on *Water and Sediment Pollution*

✉ Muhammad Bilal
muhammad.bilal@put.poznan.pl

✉ Jakub Zdarta
jakub.zdarta@put.poznan.pl

[1] Department of Chemistry, University of Agriculture Faisalabad, 38040 Faisalabad, Pakistan

[2] Department of Chemistry, The University of Lahore, Lahore, Pakistan

[3] School of Engineering and Sciences, Tecnologico de Monterrey, 64849 Monterrey, Mexico

[4] Institute of Chemical Technology and Engineering, Faculty of Chemical Technology, Poznan University of Technology, Berdychowo 4, PL 60965 Poznan, Poland

Heavy metals may be found in wastewater from several industries and human activities, including plating and electroplating, pesticides, batteries, rayon production, mining, metal rinsing, textile production, tanning, paper making, petrochemical processing, and electrolysis. Humans exposed to heavy metals tend to develop serious health issues, including damage to vital organs like the liver, heart, brain, and kidneys. They tamper with the body's natural processes, altering the outcomes. Due to their inert nature, they linger in the surroundings for a considerable time, making them a potential health hazard [2]. Polluted water exposed to heavy metals eventually makes its way into the ecosystem, posing a risk to both human physical condition and the surroundings [3]. Profound metals are potentially carcinogenic [4] and are not degradable; therefore, their presence in water in excessive quantities may be very harmful to human beings [5].

Chromium is amply used in metallurgy, pigments, catalysts, textile and leather tanning industries, electroplating processes, and wood preservation, among other applications worldwide. From the two stable chromium forms in water, Cr(III) and Cr(VI), Cr(III) is characterized by low mobility, is not toxic, and plays a role in carbohydrate metabolism. In contrast, Cr(VI) is highly mobile in water and extremely harmful, forming Cr(V/IV) intermediates by intracellular reduction and causing mutagenic and teratogenic effects. The World Health Organization (WHO) recommends a maximum level of Cr(VI) in drinking water of 50 μg L^{-1}, and the limits for Cr(VI) in wastewater go from 5 up to 500 μg L^{-1} [6].

The presence of arsenic in wastewater, groundwater and soil, due to its natural contamination, is a serious problem in many regions around the world, like China, the USA, Bangladesh, Chile, Mexico, Taiwan, Japan, Poland, Argentina, Hungary, Canada, and India [7]. Acute human arsenic poisoning may result in serious gastrointestinal problems, circulatory irregularities, hepatic collapse, or renal failure as well as lead to cancer, hyperpigmentation, and hyperkeratosis. Despite the availability of treatments for acute symptoms, no therapies exist yet for chronic exposure; as a result, preventing exposure is crucial. It has been reported in recent years that precipitation, oxidation, including advanced photocatalytic methods, coagulation, membrane filtration, adsorption, and ion exchange are among the most frequently used methods for arsenic removal [8]. Nevertheless, further work on the development of safe and financially sustainable solution for wide-scale applications is still required.

Due to its bioaccumulation and high toxicity, mercury (Hg) is considered a worldwide contaminant that threatens human health including cancer and heart diseases, and the ecosystem. It should be underlined that both, inorganic Hg as well as organic methylated Hg species (MeHg) should be considered as potentially harmful for living organisms after exposure [9]. Both natural emissions and human activities contribute significantly to mercury levels in the environment. Mercury species are common in wastewater, soil, and sewage sludge and due to their mobility and other properties might easily transfer between various clusters and enter the food chain. Released via plant respiration, geothermal activity, forest fires, soil contamination, and ocean water evaporation are only a few of the natural causes of mercury emission. Most mercury contamination comes from human activities and amounts to around 5000 tons annually. It is present all over the world. But the hypertoxicity of mercury vapors and mercury salts may injure human bodies via inhalation or ingestion [10].

Electrocoagulation (EC), adsorption utilizing natural and synthetic adsorbents, magnetic field application, enhanced corrosion processes, membranes, etc., have all been the subject matter of the current study into the removal of hazardous or heavy metal ions, as shown in Fig. 1. These reports discussed the pros and cons of a selected technique for profound metal exclusion from wastewater. There is no comprehensive picture of how wastewater resources may be cleaned of heavy metals. Therefore, the present research analyses and evaluates the methods currently used to efficiently eliminate heavy metal ions from wastewater. In addition, the elimination effectiveness, chemicals added/adsorbents, beginning attentiveness, ideal treatment pH value, and other working parameters are all critical factors in determining the best approach to take [11, 12]. This present review concentrates on the important principles involved in the photocatalytic oxidation and adsorption of heavy/hazardous metals utilizing advanced nanocomposites. The mechanism of adsorption and sources of these metals and their remediation by nanomaterials are comprehensively discussed and evaluated in this review.

Electrocoagulation

The electrodes dissolve by applying an electric current, and the pollutants are trapped as flocs, which may then be removed from the electrolytic mixture, a process known as electrochemical oxidation (EC). By dissolving the anode and hydrolyzing the released metal ions, we can weaken the charged contaminants and force them to floc together [13]. The polar moment and oxidizing power of the metal hydroxyl ions cause them to form complexes with the pollutants, ultimately leading to floc formation. Electrochemical (EC) wastewater treatment cells have a power source and electrodes submerged in a thermally protected chamber. Electrode type, electrode distance, applied current density, beginning pH, electrolyte conductivity, and treatment duration are the most influential aspects of the EC process. Accordingly, every EC research has to focus on optimizing the operational factors.

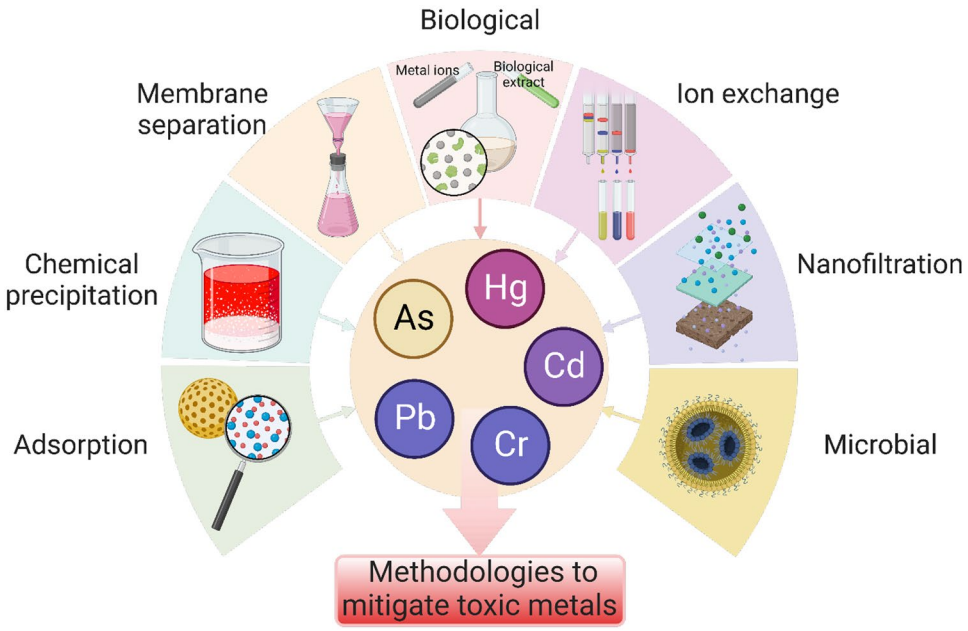

Fig. 1 Advanced water treatment methodologies for the removal of toxic metals. Created with BioRender.com and extracted under premium membership

In most cases, iron (Fe) and aluminum (Al) plates are utilized as electrodes because of their accessibility, low cost, and high removal efficiency. When an electric current is passed through the cell, the sacrificial metal electrodes dissolve, releasing metal hydroxides into the electrolyte. These hydroxides strongly attract the contaminants present in the electrolytic medium. Where *M* is the solid metal electrode and *n* is the number of ion charges, the following equations explain this process [14].

Anode

$$M_{(s)} \rightarrow M_{(aq)}n + ne^{-}$$
$$2H_2O \rightarrow 4H^{+}_{(aq)} + O_{2(g)} + 4e^{-}$$

Cathode

$$M_{(aq)}n + ne^{-} \rightarrow M_{(s)}$$
$$2H_2O(I) + 2e^{-} \rightarrow H_2 + 2OH^{-}{}_{(aq)}$$

Faraday's law is used to make estimates about the amount of metal ions released during EC reactions due to electrode dissociation. Faraday's law provides a theoretical electrode consumption number that may be used to assess EC performance and optimize its operation [15].

It is crucial to emphasize how EC significantly outperforms CC. EC's lack of moving components contributes to its ease of use and low maintenance requirements [16]. Regarding treating bilge water (oily wastewater generated inside ocean vehicles), Aswathy et al. demonstrated a significant difference in COD removal% between EC and CC. EC eliminated 78% of the COD, but only 59% was eliminated by CC. In addition, the sludge produced by EC was superior to CC in terms of acid resistance, stability, floc size, and bound water; it could be promptly separated by filtering and dewatered with less effort [17]. In addition, the necessity for chemical addition is reduced in EC since electricity drives the production of metal coagulants. However, the high cost of the power makes EC impractical in the least developed countries (LDCs). Researchers have looked at solar-powered EC-based wastewater treatment and found encouraging results [18]. Therefore, EC may further help economic and environmental sustainability in wastewater treatment by using renewable energy as a power source.

Many types of wastewaters, such as bilge water, textile wastewater, municipal wastewater, tannery wastewater, oily wastewater, urban wastewater, mineral processing wastewater, metalworking fluid wastewater, laundry wastewater, and palm oil mill effluents (POME), have been studied in EC treatment [19–22]. It is noteworthy that EC treatment is over 85% effective in removing pollutants from various wastewater types, establishing its credibility as a viable alternative treatment technique. EC is one of the most environmentally friendly methods of treating wastewater since it is efficient at removing pollutants, has a small footprint, does not need a lot of chemicals, is simple to set up, and produces no dangerous waste products. However, EC has inherent limits in purifying water to the purity level of reuse, and the EC process degrades sacrificial electrodes with time, necessitating periodic electrode replacement. As a result, there is a lot of opportunity for development in the use of EC technology, particularly in terms of optimizing operating parameters to achieve the highest possible purity and yield.

Heavy/Hazardous Metals in Wastewater

Chromium (Cr(III), Cr(VI)) as Major Textile Effluent

Gervas et al. [23] demonstrated that heavy metals were recognized as significant pollutants intimidating the physical condition of living organisms and distressing the surroundings. The increasing knowledge on the toxicity of profound metals has been responsible for amplifying the attention in contamination treatment. Industrial wastes were considered the main contaminants among all industrialized effluents and the bulky challenger of chromium ions contamination to the surroundings. Toxic metal (Hg, Cr, and As) concentration in surface water bodies is compared in Table 1. From different industries, about 2000 mg L^{-1} to 5000 mg L^{-1} chromium ion absorption evaded into the surroundings, far superior to the suggested permitted expulsion limits. Chromium(III) was one of the contaminants present in normal waters by a range of industrial effluents in the leather industry, fabric, metal, and electroplating dying industries. During tanning, only 60% of the functional chromium salt was used, and the leftover was sent to a purification plant, where the salts ended up in the mud. This was the major ecological crisis in industries. Ahmed et al. [24] considered that using cement dust and lime, chemical precipitation of trivalent chromium was conceded. The actinomycetes strain of *Kitasatosporia* sp. was used in microcosm analysis for hexavalent chromium bio-elimination.

Parameters like the variety of permeable medium inoculums range, culture situation, and flow rate were analyzed. The precipitated trivalent chromium was improved from the chemical rainfall phase $f_{x4}d_7$ recycled in the leather production industry. Mutual chemical, organic handling of chromium-contaminated wastewater became more profitable and ecologically friendly than biological or physio-chemical management alone. Minsa et al. [29] proposed a substitute method for recovering and removing chromium(III) from wastewater through elemental rainfall with sodium hydroxide, magnesium oxide, and calcium hydroxide. The special effects of pH, settle the point, stirring time, and mud quantity was evaluated in the consignment examination. However, chromium concentration was detected by using flame atomic absorption spectrometry. The consequences demonstrated that elimination efficiencies of the precipitating agents such as sodium hydroxide, magnesium oxide, and calcium hydroxide were 99.97%, 99.98%, and 99.97%, respectively. However, there was a significant disparity in slush quantity of sodium hydroxide, magnesium oxide, and calcium hydroxide were 590 mL, 85 mL, and 412 mL, respectively. Magnesium oxide was considered to be a better precipitating chemical for the elimination and revival of chromium from wastewater. Henryk et al. [30] demonstrated that the batch adsorption method was evaluated to exclude trivalent and hexavalent chromium ions from aqueous mixtures utilizing coconut fibre and Canadian peat. The highest adsorption for peat was 8.02 mg g^{-1} for Cr(VI) and 18.75 mg g^{-1} for Cr(III), while the charge for twine was considerably elevated and reached 19.21 mg g^{-1} for Cr(III) and 9.54 mg g^{-1} for hexavalent chromium.

Zhao et al. [31] demonstrated that hexavalent chromium released from fabric fading, tanneries, metallurgical chromite ore smelting, and electroplating is extremely diffusive and carcinogenic. Several technologies have been applied to take away hexavalent chromium from wastewater. Consequences demonstrated that biochars had amazingly discerning adsorption of hexavalent chromium. X-ray absorption close to the border and X-ray photoelectron spectrum exposed that hexavalent chromium was condensed to trivalent chromium. Jobby et al. [32] recognized that all the adsorption was carried out at pH near seven, which was dissimilar from the preceding analysis that hexavalent chromium could only be condensed at 2–4 pH. The biochar with ecological unrelenting free radicals exposed an extremely discerning elimination of hexavalent chromium, which had implications for the remediation of contaminated water. In an aqueous solution, hexavalent chromium could appear as numerous species such as CrO_4 and $HCrO_4^-$. This allocation was dependent on pH of the solution, overall chromium absorption, the redox potential, the existence of reducing and oxidizing compounds, kinetics of the reducing and oxidizing reactions and the redox potential. If the pH of the mixture was greater than 7, CrO_4 was the only accessible ion independent of hexavalent chromium absorption. Whereas $HCrO_4^-$ was the significant species where the pH range was 1–6. However, the chromium absorption in these effluents varied between 2 and 5 g L^{-1}, which was more effective than the permitted limit of 2

Table 1 Comparison of toxic metals (Hg, Cr, and As) concentration in surface water bodies

Hazardous metal	Safe limit for drinkable water (mg L^{-1})	Concentration in surface water bodies from industrial effluents (mg L^{-1})	Hazard intensity score	Ref.
Mercury	1.45	1.5	1458	
Chromium	4.47	366.9	895	[28]
Arsenic	83.7	6662.5	1674	

mg L^{-1}. Bhati et al. [33] reported that hexavalent chromium was a poisonous and non-recyclable contaminant that results from frequent industrialized processes and could cause an imperative ecological scratch if not detached from industrial waste. However, it could be condensed to trivalent chromium that was less deadly and could be eagerly precipitated out and disconnected. There was a quick and simplistic distinct stair method for producing phosphorus nitrogen-doped incandescent carbon dots employing a familial microwave as an impending photocatalytic object. Over ordinary light, straightforward photocatalytic research exposed to the nitrogen phosphorus-doped luminous carbon dots were highly proficient in the quantitative decline of chromium(VI) to chromium(III) in artificially contaminated water in a linear arrangement from 10 to 2000 ppm by raising the sunlight representing nitrogen phosphorus doped luminous carbon dots as an impending photocatalysts substance for hexavalent chromium water management.

Arsenic(III) Contamination in Water

Mishra et al. [34] reported that arsenic contamination was one of the world's chief problems corresponding to transferable water. Several arsenic elimination methods included adsorption, precipitation, solvent extraction, ion exchange foam flotation, nanofiltration, and natural appropriation. Among all the accessible ways, adsorption was estimated as the most favorable method to compact with the crisis. Trivalent iron oxides had revealed incredible impending adsorption of arsenic in the form of these oxides had higher sorption empathy toward both trivalent and pentavalent arsenic forms. CuO nanomaterials have been established as an excellent, efficient adsorbent for arsenic elimination from an aqueous mixture.

In comparison, trivalent arsenic elimination analysis was performed by contributing a standard mixture of 100 mg L^{-1} absorptions organized by mixing arsenic trioxide in NaOH by gravimetry. Navarathna et al. [35] demonstrated that magnetic Fe_3O_4-Douglas biochar composites were synthesized with almost 29.2% weight. Tri-iron tetra oxides are used to treat triarsenic-infected water. The toxicity of triarsenic was considerably higher than pentavalent arsenic and extra hard to eliminate from water. Exclusion effectiveness was optimized versus pH, initial concentration and contact point. The composite condensed arsenic absorptions lower the protected range of 0.2 mg L^{-1} for industrial waste ejection. X-ray photoelectron spectroscopic analysis revealed that trivalent arsenic and less poisonous pentavalent arsenic on tri-iron tetraoxide surfaces represent adsorbed trivalent arsenic oxidation by their contact with oxygen and possibly dissolved tri-iron. Bullen et al. [36] observed that TiO_2–Fe_2O_3 composites revealed the immense potential for the exclusion of triarsenic from drinking water with the higher adsorption aptitude of iron oxides towards the arsenic(V) consequently formed. Turkmen et al. [37] revealed that extensive arsenic-impure water contact and intake led to several neurological disorders, skin lesions, and cancer. The arsenic ion infectivity exists mainly in the inorganic ways of trivalent and pentavalent arsenic in an aqueous system where it was more tricky to remove trivalent arsenic than pentavalent arsenic. Arsenic-stamped magnetic nanoparticles were prepared using a molecular imprinting way in the existence of iron oxide for trivalent arsenic and pentavalent arsenic adsorption. To establish the highest adsorption situation, arsenic elimination analysis with arsenic-stamped magnetic nanoparticles was determined by using numerous parameters such as pH, temperature, concentration, and point-dependent alteration. Arsenic stamped magnetic nanoparticles pooled with the molecular imprinting practice had been effectively synthesized as highly efficient materials for high selectivity of trivalent and pentavalent arsenic elimination. As a result of breaking As-O bonds and reactivity with oxygen, arsenic species are further reduced and distributed throughout the thin iron oxide layer, generating As-Fe bonds. nZVI has As(0), As(III), and As(V) after As(III) adsorption. As(III) was detected in the iron oxide layer, although As(III) and As(V) were spread throughout the shell. As(0) was identified between Fe(0) and iron oxide [38]. Figure 2 shows As(III) adsorption on nZVI nanoparticles.

Mercury Contamination in Water

Gworek et al. [39] observed that mercury infectivity in the water had been a problem for living organisms' surroundings and physical conditions. In the surrounding aquatic, mercury exists in numerous ways depending on the oxidation-reduction situation. In oceanic waters, mercury mostly existed in the

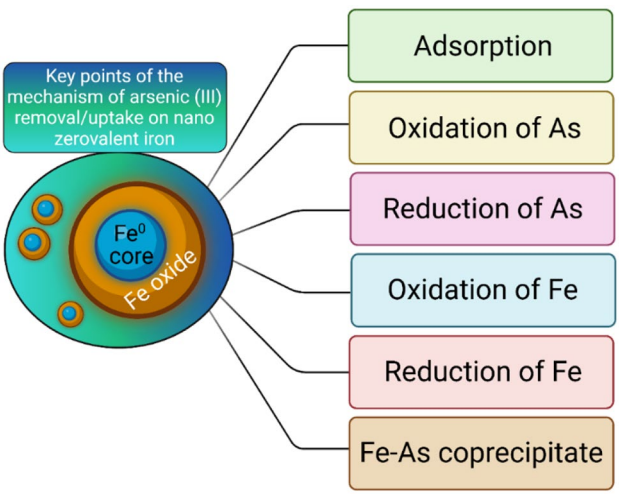

Fig. 2 Adsorption mechanism of arsenic(III) on nano zerovalent iron. Created with BioRender.com and extracted under premium membership

forms of Hg^0, Hg^{2+}, MeHg, and diMeHg and colloidal shape. In marine water, mercury combines with chlorine to form $HgCl_3$ and $HgCl_4$ to a better amount than oxides. Similarly, in freshwaters, it had been confirmed that Hg^{2+} combines with chlorine to form mercury halides. These complexes did not undergo the diminution and methylation method. Verma et al. [40] studied that mercury was a liquid metal known as quicksilver.

The intensity of mercury pollution was in a variety of water bodies, and this infected water was issued chiefly for consumption and agricultural reason. The chief resource of mercury contagion could be sewage, industrial, natural, agricultural, medical goods, sediments, cement plants, fly ashes, etc. [41]. Mercury was an extremely venomous metal which was frequently present in the surrounding. The poisonous overdose consequences of mercury were on the thyroid gland, neurological, reproductive, and gastrointestinal tract, which sometimes would lead to death. Typically, individual contact with mercury was responsible for contamination through gassing mercury through dental amalgamation and ingestion of impure fish. Wang et al. [42] offered that mercury pollution was critical apprehension worldwide due to its poisonous effect on human physical condition. Among non-living mercury, Hg^{2+} had been confirmed to be a significant deadly element that could be responsible for affecting the lung and kidneys. The chief descent of elemental mercury was authentication to soil or an aqueous environment after corrosion to divalent mercury. Exclusion technologies involve the method of desorption, adsorption, reduction, and oxidation. These technologies' chief endeavor was to remove mercury from the impure area or distort poisonous mercury species into fewer venomous ones. Slimani et al. [43] exposed mercury as a toxic pollutant in most marine ecosystems. Higher absorptions posed severe intimidation to organisms and the human physical condition. The initial analysis exposed that some of the sites were highly impure, where mercury absorptions were over 5 μg g^{-1}.

Fu et al. [44] demonstrated that carbon quantum dots could remove mercury ions from an aqueous solution. This cutting-edge technology can eliminate mercury ions from the atmosphere and detect them. The initial mercury concentration was 100 ppm, and the adsorption experiment was conducted at a constant temperature and under neutral circumstances. The detection threshold is now closer to 10 ppb, which meets drinking water requirements. The maximum adsorption capacity was 3.33 mg of mercury per 1 g of the sorbent, more significant than AC (active carbon), graphene, and carbon nanotubes. Under UV irradiation, fluorescence emission is followed by fluorescence quenching due to the creation of the CQD-Hg^{2+} complex ion and subsequently by the sedimentation of Hg-based spheres due to adsorption saturation (Fig. 3).

Main Sources of Heavy/Hazardous Metal Pollutants

Zhou et al. [45] demonstrated that with time, profound metal contamination in groundwater had distorted from solo metal contamination to mixed metal effluence. Profound metal absorptions in water and the quantity of heavy metals with absorption over the verge restrictions. Manufacturing, mining, pesticide, fertilizer, and pesticide use were the foremost resources in North America. In contrast, four manufacturing sources, mining, fertilizer, rock corrosion, pesticide use, and waste discharge, were responsible for the bulk of deep metal contamination in the pond water bodies and streams. Moreover, implementing meticulous values on metal discharge and recycling metals from wastewater was effective for scheming

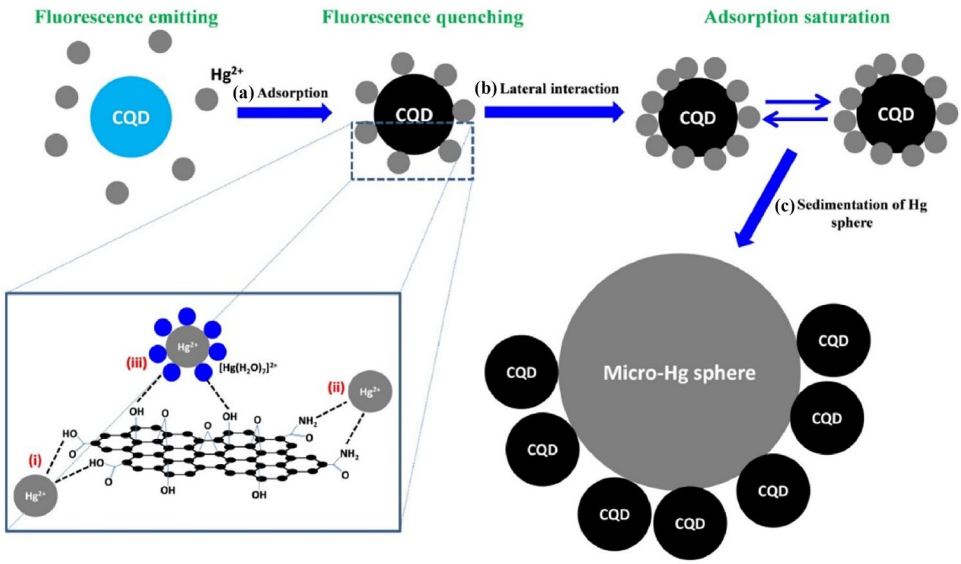

Fig. 3 Five-step mechanism of adsorption on CQD for mercury removal. Reprinted from Ref. [44] with permission from Elsevier. License Number: 5435991409400

heavy metal resource contamination. Marrugo et al. [46] recognized that the continuation of metals in farming soils from anthropogenic actions like drawing out and agricultural usage of metals and metal-comprising compounds was a prospective hazard for the individual physical condition through the provisions chain. Metal content was the product of metals arising from individual behavior and ordinary processes. Ertani et al. [47] found that the bulk of chromium in oxidation states ranges from zero to six in soils. Still, the main constant and common types were chromium(0), chromium(III), and chromium(VI) forms. Chromium was referred to as a significant contaminant discharged into the surroundings by industries. Contagion of soils and groundwater due to the use of this metal in a variety of anthropic actions was a universal crisis that had been analyzed by the scientific area for years and was still a recent matter. The leather and tannery industries in meticulous were mainly accountable for the creek of this metal into the atmosphere. Shahid et al. [48] proposed that arsenic contagion was a worldwide ecological, farming, and communal health matter due to its extremely poisonous and carcinogenic character. Arsenic was classified as one of the primary lethal and carcinogenic contaminants by numerous international and national ecological and health organizations and presently poses a rigorous hazard to the human and environmental physical condition, particularly in groundwater where it was used for ingestion of water materials and has caused unfavorable impacts on individual physical condition. Arsenic was discharged into the surroundings in various ways like weathering of parent stuff, volcanic eruptions, and the expulsion of geothermal waters. Economou et al. [58] found that chromium and arsenic were extensively dispersed due to the rising challenges of ordinary and anthropogenic activities in the surroundings. Chromium and arsenic were present in earth and groundwater due to geogenic course and anthropogenic behavior like melting operations, fossil fuel burning arsenic chromium-based agrochemicals, fertilizers, textile dyes, and straight discarding of public and manufacturing waste [68]. The concentration limit of heavy metals, which are deadly for humans, plants, and animals, has been discussed in Table 2.

Profound metals were one of the primary contaminants that supply the increasing ecological contamination crisis, principally involved in receptive environmental areas through manufacturing wastewater and manure of frequent industries. Malek et al. [88] proposed that the existence of minor quantities of a microgram or nanogram per liter of this contaminant exhibited poisonous special effects. The kinds and statistics of contaminants were massive. The most common non-living micropollutants integrated transition and heavy metals were chromium, mercury, arsenic, and pollutants that came in ordinary water from various resources. Industrial and domestic wastes are the chief contributors of various contaminants, as shown in Fig. 4. Industrial and municipalities used almost 30% of the internationally available renewable freshwater. Agricultural actions resulted in the use of vast quantities of pesticides which provoked the trouble of poisonous microcontaminants in water. Gasoline, oil spills, and anthropogenic resources of physically occurring geogenic toxic chemicals like heavy metals and metalloids also caused considerable harm. There were physically formed common micro pollutants consisting of odor and foul taste [89]. There were several examples of dangerous dissipate sites which were accountable for poisonous chemicals in flowing into mercury contamination was extensive and happened through a diversity of natural and anthropogenic resources. These included oceanic and volcanic erosion, coal and gold extraction, solid dissipate burning, chemical development, and fossil fuel burning.

Adsorption Process for Water Remediation

Park et al. [90] demonstrated that water contamination by profound metal emissions from different industrial wastewater was labelled as a universal crisis. During current years, most heavy metal forms had poisonous special effects on organisms and accumulated in bodies. Among various management technologies, adsorption was a quick and general technique for treating profound metals with effectiveness and lower cost. A variety of sorbents, including ordinary materials and manufactured goods, had been urbanized and established those carbon-based adsorbents recognized as the majority charge effectual for eliminating organic and inorganic contaminants from wastewater. While activated carbon was perfect for excluding pollutants from water, it was expensive to form, whereas sustainable biochar required less speculation. Classic biochar was less carbonized, and

Table 2 Various concentration limit of heavy metals for humans, plants, and animals

Metals	Concentration limit harmful to human (mg kg^{-1})	Concentration limits harmful to plants (mg kg^{-1})	Concentration limit harmful to animals (mg kg^{-1})	Ref.
Chromium	1900–3300	0.17–1.74	4.3	[69–71]
Arsenic	2.5–33	25–85	5.6	[72–74]
Mercury	0.5–10	3.8–9.1	> 0.5	[75, 76, 87]

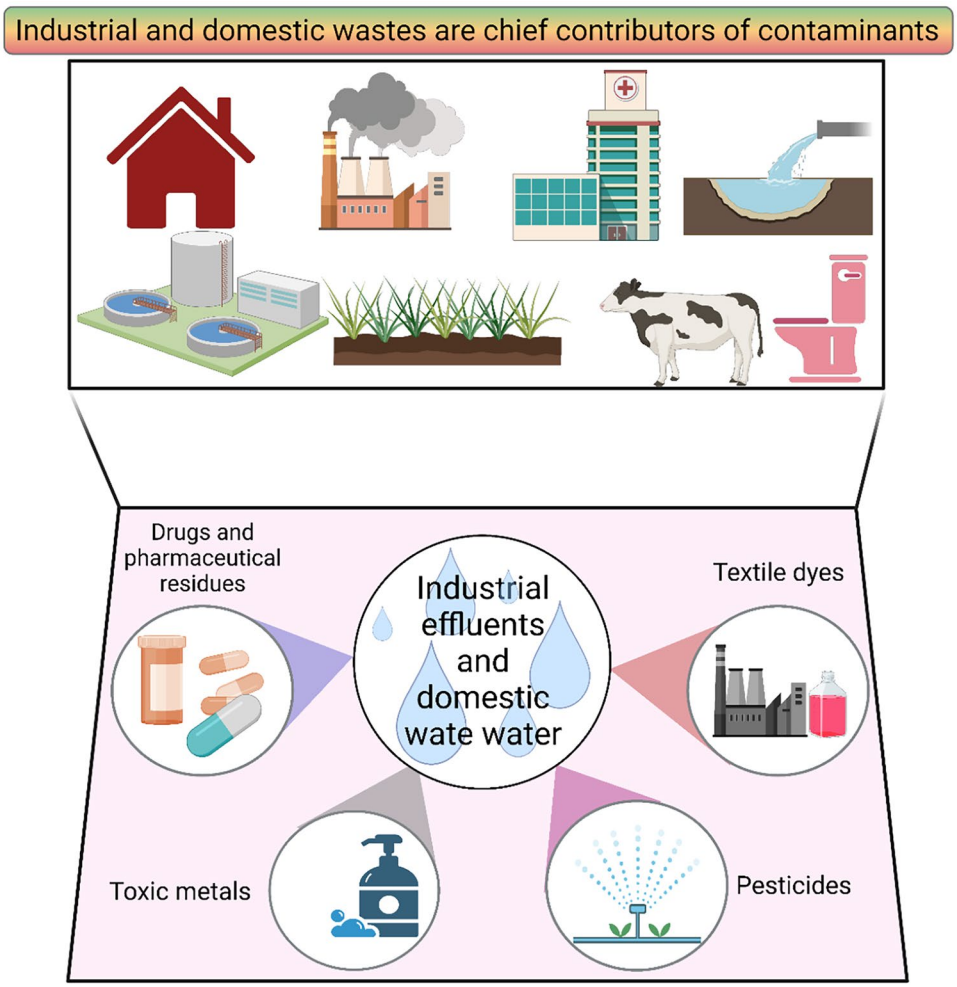

Fig. 4 Various industrial and domestic wastes, as the chief contributors to numerous contaminants. Created with BioRender.com and extracted under premium membership

additional oxygen and hydrogen remained in its arrangement than activated carbon. It was a low-charge adsorbent which had lately received amplified concentration due to its numerous impending ecological applications and settlement. Using biochar as a sorbent to remove wastewater comprising profound metals was a rising and talented skill. Biochars had derivatives from plant residues, and farming wastes had been experienced for their capacities to sorb a variety of profound metals. Bode et al. [91] found that the adsorption procedure had been measured as the cheapest and most straightforward method for excluding toxic metals from an aqueous mixture. The recital of the adsorption system was mainly reliant on the feature of adsorbents. Therefore, the construction of materials on the nanoscale was convenient for the adsorption technique. The electrospinning procedure was one of the technologies that had been engaged to create polyacrylonitrile nanofibres. Furthermore, polyacrylonitrile nanofiber planes had also been chemically customized so as to commence the chelating groups like carboxyl and amine and imines. Customized polyacrylonitrile nanofibers were measured as fine adsorbents and had been used to abolish poisonous metals such as mercury, chromium, and copper in dissimilar ionic states from their aqueous mixture. The ease of restriction of metal precise ligands on polyacrylonitrile nanofibers had been of immense concern in discerning the removal of metal ions from their aqueous mixture. Also, poisonous metals adsorbed on customized polyacrylonitrile nanofibers could be improved through a desorption course using acids or bases of a variety of absorptions.

Mechanism of Adsorption

Gendy et al. [92] found that covalent organic frameworks could considerably eliminate profound metals due to their high adsorption capability, higher surface area, recyclability, and permeable arrangement. The functional group and substance arrangement significantly enhanced the elimination effectiveness of profound metals. Xu et al. [93] proposed that oxides of iron nanoparticles had usually been used to eliminate aqueous arsenic with an adsorptive ability for diverse Fe_2O_3 and Fe_3O_4 of 5.99 mg g^{-1}.

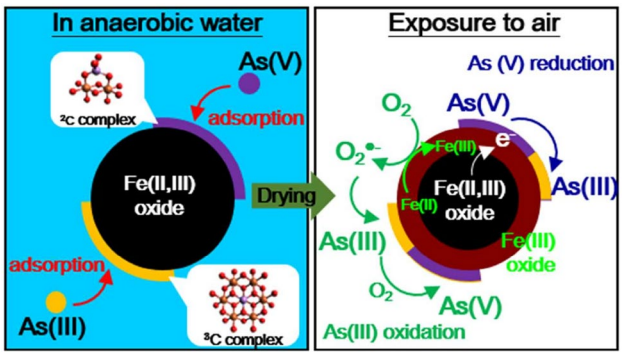

Fig. 5 Arsenic adsorption mechanism on magnetic particles in aerobic water and anaerobic water. Reprinted from Ref. [95] with permission from the American Chemical Society

The highest adsorptive powers of trivalent and pentavalent arsenic by the carbon nanotube-based oxides of iron were 24.05 mg g^{-1} and 47.41 mg g^{-1}, correspondingly. Since the oxidation time of trivalent arsenic by tetravalent manganese complexes was considerably superior to that by trivalent iron complexes, GO-$MnFe_2O_4$ nanohybrids were fictional. The adsorptive abilities of trivalent and pentavalent arsenic by GO-$MnFe_2O_4$ nanohybrids were enhanced to 146 mg g^{-1} and 207 mg g^{-1} correspondingly, which was superior to GO-nanoparticles in the absence of tetravalent manganese complexes. The Langmuir isotherm replica was generally used for monolayer adsorption from where most adsorption sites had equivalent associations toward the adsorbate.

In contrast, the Freundlich isotherm form was used to explain a diverse chemisorption procedure in which the plane was not vigorously consistent. The Redlich-Peterson isotherm method was a mixture of the Langmuir and Freundlich methods with values β was 0–1 order. If the value of αCeβ was superior to 1, then it could be almost by the Freundlich equation, while if β = 1, the equation could be almost by the Langmuir isotherm method. The Dubinin Radushkevich isotherm model was frequently involved in examining the kind of adsorption procedure [94]. Most of the working graphene nanomaterials and carbon nanotubes showed enhanced robustness with the Langmuir isotherm method and the adsorptive abilities of the graphene-based nanomaterials and carbon nanotubes for the elimination of a variety of aqueous heavy metals.

Liu et al. [38] found that adsorption of arsenic onto MNPs is endothermic. It was hypothesized that As(V) adsorption on MNPs proceeds via the formation of bidentate binuclear corner-sharing complexes (Fig. 5) [95]. Whereas Albatrni et al. [96] demonstrated numerous attempts to adsorb mercury and other metal ions from wastewater using stumpy charge bio adsorbents. Table 3 represents recent studies on removing chromium, mercury, and arsenic by the adsorption process.

Carbon-based Nanocomposites for Removing Industrial Pollutants

Arsenic remediation relies heavily on using effective adsorbents that have a high removal rate and can be reused. Permeable magnetic nanocomposite for effective arsenic elimination was

Table 3 Removal of industrial effluents using the adsorption process

Composite	Efficiency (%)	Pollutant	Catalyst dosage	Pollutant dosage	Synthetic method	pH	Ref.
Titanate nanotube composite	60.1	Chromium(III), Chromium(VI)	Dosage 0.16 g L^{-1}	10 mg L^{-1}	Hydrothermal method	5.0	[97]
Zirconium dioxide-loaded montmorillonite composites	92	Chromium (III)	0.5 g	10 mg L^{-1}	Ion exchange process	7–8	[98]
Starch-based nanocomposite	95.5	Mercury	192 mg g^{-1}	10–150 mg L^{-1}	Batch adsorption method	6	[99]
polypyrrole (PPy)/SBA-15 nanocomposite	68.3	Mercury	1 g L^{-1}	200 mg g^{-1}	Batch adsorption method	8	[100]
Titanium carbide magnetic nanocomposite	98.9	Mercury	0.025 g L^{-1}	10 mg L^{-1}	Batch adsorption method	6	[101]
Zeolite silver nanocomposites	6.5	Mercury	20.5–22.3 mg g^{-1}	10–500 mg L^{-1}	Hydrothermal alkaline method	2–6	[102]
Magnetic bio-composite	95.6	Mercury	0.1 M	0.006 mg L^{-1}	Co-precipitation method	6	[103]
Magnetic nanocomposite	-	Arsenic(III)	0.60 mg mL^{-1}	1.280–0.210 mg L^{-1}	Sol–gel method	7	[104]
Metal–organic framework-graphene oxide nanocomposite	3	Arsenic(III)	0.2–3.0 g L^{-1}	10–110 mg L^{-1}	Batch adsorption method	2–11	[105]
Magnetic Fe3O4@CuO nanocomposite	-	Arsenic(III)	120 mg L^{-1}	70.36 mg g^{-1}	Modified Hummers method	3–9	[106]

synthesized by the straightforward one-pot co-precipitation of Fe_3O_4 NPs on permeable halloysite nanotubes/C (HNTs/C) manufactured utilizing discarded polyurethane fluff. After adhering to the carbonized phenolic resin, HNTs were injected into the polyurethane foam pores to create the nanocomposites' framework. The nanocomposites of HNTs, carbon, and iron oxide nanoparticles (NPs) were generated by the uniform distribution of NPs throughout the framework. It was found that the optimized HNTs/C/Fe_3O_4 had a very high removal rate (> 98% arsenic was eliminated after 10 min), high elimination efficiency, and excellent regeneration capacity [107].

Scientists created a unique material called Fe/Mn-C layered twice hydroxide compound (Fe/Mn-C-LDH) to eliminate arsenic in water. The effectiveness of the composite at removing arsenic ions was investigated using batch studies. Adsorption capacities of 46.47 mg g^{-1} for As(III) and 37.84 mg g^{-1} for As(V) at 318 K were observed for Fe/Mn-C-LDH. Furthermore, the release of iron and manganese during the arsenic adsorption process was studied. The Fe/Mn-C-LDH was more stable than the Fe/Mn-layer twofold hydroxide (Fe/Mn-LDH), with less Mn^{2+} and Fe^{3+} being released under the same conditions. According to the BET data, the adsorption of arsenic(III) and arsenic(V) onto Fe–Mn-C-LDH reduced its specific surface area [108]. Among both composites, HNTs/C/Fe_3O_4 showed the best performance because of their unique heterojunction. A unique porous halloysite nanotube structure resulted in the enhanced photocatalytic performance of the composite. In general, well developed, and highly porous structure if halloysite materials facilitates their use in various roles in the removal of hazardous ions. A detailed comparison of various carbon-based nanomaterials for removal of textile effluents has been presented in Table 4.

Polymeric-based Nanocomposites for Efficient Adsorption of Industrial Pollutants

The goal of designing and synthesizing adsorbents for the effectual elimination of mercury ions from wastewater using a simple and cost-effective technique is appealing. Mercury may be removed from water using a unique sulfur-rich microporous polymer (sulfur content of 31.4 wt%), which has an excellent surface area and a higher meditation of sulfur atoms that could be quickly accessed. Significant binding affinity, high adsorption capacities, rapid adsorption kinetics, and excellent recyclability were all shown by the as-produced polymer (SMP) for Hg^{2+}. SMP has an adsorption capability of 595.2 mg g^{-1}. In addition, SMP can eliminate Hg^{2+} traces from water at concentrations below the EPA (Environmental Protection Agency) drinking water limit of 2 ppb from 200 ppb in only 3 min [116].

Ionic fluid (tricapryl methylammonium chloride (Aliquat 336)) was utilized to produce polymer inclusion membranes (PIMs) for the selective and facilitated transfer of chromium ions. PIMs were optimized for CTA (cellulose triacetate) to PBAT (poly(butylene adipate-co-terephthalate)) ratio. Several methodologies were used to study the presence of membrane masterpiece and ionic fluid on PIM characteristics. Infrared research revealed intermolecular connections between the hydroxyl groups of CTA and PBAT and the negatively charged carboxyl groups of CTA and Aliquat 336. Aliquat 336 and PBAT changed the membrane's hydrophobic/hydrophilic characteristics. PIM with equal amounts of CTA and PBAT (35/35 wt%/wt%) and 30% Aliquat 336 was carried out for Cr(VI) ions transport tests. This PIM transfers > 99% chromium in six hours and collects 5% with

Table 4 Carbon-based nanocomposites for effective removal of textile effluents

Composite	Efficiency (%)	Pollutant	Catalyst dosage	Pollutant dosage	Synthetic method	pH	Ref.
Pd-GO	90	Chromium(VI)	0.05 mM	2.0 mM	-	3–4	[109]
Acid-modified activated carbon nanomaterial	96	Chromium(VI)	50 g L^{-1}	1 mg L^{-1}	Hydrothermal method	3	[110]
Longan seed-activated carbon	63	Chromium(VI)	2 g L^{-1}	100 mg L^{-1}	Hydrothermal method	3	[110]
Magnetize Go from cellulose-based graphite	-	Chromium(VI)	3.19 mg g^{-1}	10 mg L^{-1}	-	2	[111]
Fe_3O_4@2D-CF composite	-	Arsenic(III)	57.47 mg g^{-1}	52.6 emu g^{-1}	Facile one-pot method	-	[112]
Carbon-based adsorbant C-NRs/$Fe(OH)_3$	51	Arsenic(III)	1 g L^{-1}	100 mg L^{-1}	-	3	[113]
HNTs-C-Fe_3O_4	99	Arsenic(III)	5 mg L^{-1}	2 mg L^{-1}	Batch method	6	[107]
Commercial activated carbon	-	Arsenic(III)	0.29 mg g^{-1}	0.1 mg g^{-1}	Template method	-	[114]
Fe/Mn-C layered double hydroxide composite	98.2	Arsenic(III)	0.03 g	46.47 mg g^{-1}	Adsorption experiment	> 3	[108]
Biochar-based activated carbon	90	Mercury	10 mg L^{-1}	200 µg L^{-1}	Slow pyrolysis method	7	[115]

high initial flux. Blend PIMs with condensed extractant substance and no plasticizer transfer Cr more selectively than usual PIMs. Long-term (> 120 h) transport studies confirmed the mix PIMs' stability [117]. The unique sulfur-rich microporous polymer showed a large surface area due to the polymer's intrinsic sulfur content, which resulted in high adsorption capacity and high adsorption kinetics for metal ions as compared to polymer insertion membranes relying on CTA/PBAT blend consisting of Aliquot 336. A detailed comparison of various polymer-based nanomaterials has been presented in Table 5.

Semiconductor-based Nano-heterojunctions for Adsorption of Cr, As, and Hg

Using layer-by-layer technology, WO_3 nanostructures were distorted by doping them employing iron, and then these nanoparticles were utilized as photocatalytic precursors in a membrane made of polyethersulfone (PES). The psychoanalysis of UV–vis diffuse reflectance spectroscopy (UV–vis/DRS) suggests that doping WO_3 nanoparticles with Fe impurity might increase their photocatalytic activity. The innovative photocatalytic membranes accomplished the batch mode and filter system, taking away (Cr(VI)) ions. Under visible-light irradiation, the new photocatalytic membranes were demonstrated to remove Cr(VI) ions effectively and to improve the feasibility of the process that leads to reduce in its costs. The rebuff of chromium at feed concentrations of 5 mg L^{-1}, 25 mg L^{-1}, and 50 mg L^{-1} was augmented from 21%, 17%, and 9% for efficient PES to 56.3%, 41.6%, and 30.1% for the PES/(CHI-ALG)3.5 casing and 99.2%, 92.1%, and 78.1% for the PES/(CHI-ALG)3.5/Fe0@WO_3 covering [130].

Using a variety of WO_3_TiO_2 semiconductors easily generated using a sol–gel process with WO_3 concentration in the array of 1–5 wt%, the photocatalytic corrosion of arsenite to arsenate in aqueous solution was investigated. Over UV

Table 5 Polymer-based nanocomposites for effective removal of textile effluents

Composite	Efficiency (%)	Pollutant	Catalyst dosage	Pollutant dosage	Synthetic method	pH	Ref.
Calixarene-based polymer inclusion membrane	97.6	Chromium(VI)	1.75 mL	0.1 M	-	5	[118]
Microchannel-embedded metal–carbon–polymer nanocomposite	75	Chromium(VI)	80 mg g^{-1}	50 mg L^{-1}	Batch adsorption experiment	1.2	[119]
Polymer functionalized nanocomposites	82	Chromium(VI)	100 mg L^{-1}	50 mg L^{-1}	In situ synthesis		[120]
Chitosan composite microbead	68.1	Chromium(III)	0.05–0.25 g	2–12 mg L^{-1}	Bleaching treatment	3.0–6.0	[121]
Polymer inclusion membranes based on CTA/PBAT blend containing Aliquat 336	99	Chromium(VI)	5 mg	10 mg L^{-1}	-	-	[117]
Electrospinning of polymeric nanofiber (nylon 6,6/graphene oxide)	89.2	Chromium(VI)	0.2 g L^{-1}	47.17 mg g^{-1}	Batch adsorption experiment	2	[122]
Microwave-assisted synthesis of imprinted polymer	-	Arsenic(III)	1 mg L^{-1}	3.3 mg L^{-1}	Adsorption method	7	[123]
Polymer-based hydrated iron oxide adsorbent	94	Arsenic(III)	25 mg L^{-1}	50 mg L^{-1}	Anion exchange resin method	2–3	[124]
Oxidant Functionalised Cationic Polymer Hydrogel	85	Arsenic (III)	263 mg g^{-1}	200 mg g^{-1}	Ion exchange method	-	[125]
MOF/polymer/graphene oxide composite	> 90	Arsenic(III)	180 mg g^{-1}	50 mg L^{-1}	Adsorption method	3–12	[126]
Sulfur-rich microporous polymer	99.7	Mercury	595.2 mg g^{-1}	-	Adsorption kinetic method	1	[116]
Triazine-based N-rich porous covalent organic polymer	99.9	Mercury	1630 mg/g	10 mg L^{-1}	Adsorption kinetic method	-	[127]
Modified ion-imprinted chitosan particles	> 95	Mercury	50–500 mg L^{-1}	1 g L^{-1}	Adsorption kinetic method	5–7	[128]
Thiophenol-thiophene polymer	99	Mercury	-	1000 mg L^{-1}	Langmuir adsorption isotherm		[129]

light, the combined materials exhibited higher photocatalytic activity towards As(III) photo-oxidation than did the separate components. Molybdenum blue was used to calculate the concentration of trivalent and pentavalent arsenic species in the irradiation solution. Photocurrent and electrical impedance spectroscopy (EIS) studies confirmed photoinduced carrier separation efficacy. Under UV irradiation, 99% of trivalent arsenic was transformed to pentavalent arsenic in the first 25 min when the twofold oxide 3%WO_3_TiO_2 (TW_3) was employed. Enhanced charge partition owing to the relocation of photoproduced holes in TW_3 photocatalyst may account for the heterostructures' better photocatalytic efficacy. A good technique for the photo-oxidation of trivalent arsenic over TW_3 new catalyst has been presented, and it is based on the electric crowd organization of WO_3 and TiO_2 [131]. A detailed comparison of various semiconductor-based nanomaterials has been in Table 6.

Photocatalytic Reduction of Chromium(VI) to Chromium(III)

In the presence of organics in natural and wastewaters, studies on the photocatalytic reduction of heavy metals like chromium(VI) have generally indicated an increase rate of chromium(VI) photocatalytic reduction [141, 142]. Most of these experiments made use of TiO_2 or a TiO_2-based photocatalyst. Despite its potential, TiO_2 is limited in its use due to its relatively high band gap since it can only respond to UV irradiation, which makes up only 4% of solar energy [143–146]. Hexavalent chromium(Cr(VI)) ion presence in water and wastewater has been recognized as a serious concern due to its high toxicity for human, animal, plant, and biological systems [147, 148]. Chromium and its derivatives are discharged into water sources from several industrial processes. These processes include glass staining, electroplating, metallurgy, leather, organic synthesis, textile dying, and wood preservation. The World Health Organization (WHO) recommends that Cr(VI) ion levels in drinking water not exceed 0.05 ppm and surface water levels not exceed 0.1 ppm. From this vantage point, various research projects have investigated the viability of removing Cr(VI) from water and wastewater through multiple processes. Cui et al. [149] looked into the effect of TiO_2-rGH adsorption and photocatalysis on the removal of hexavalent chromium from an aqueous solution. TiO_2-rGH could eliminate 5 ppm Cr(VI) from a solution exposed to UV light for only 30 min. Using a g-C_3N_4/graphene hydrogel system, Liang et al. [150] found that 80% of Cr(VI) ions were adsorbed by composite within 0.5 h. Membrane technology stands out among alternatives because of its low energy consumption, simplicity of operation, the relatively inexpensive cost in the long term, and outstanding efficiency in eliminating Cr(VI). Chromium may exist as either Cr(III) or Cr(VI) in aqueous solutions. As a result of the increased toxicity of Cr(VI) ions compared to Cr(III) ions, recent efforts have focused on converting

Table 6 Semiconductor-based nanocomposites for effective removal of textile effluents

Composite	Efficiency (%)	Pollutant	Catalyst dosage	Pollutant dosage	Synthetic method	pH	Ref.
Iron-doped ZnS	60	Chromium(VI)	1 g L^{-1}	50 µg L^{-1}	Hydrothermal method	7	[132]
PbS QDs	-	Chromium(VI)	0.1 µM	1 µM	-	6.6	[133]
Fe^0@WO_3	99.2	Chromium(VI)	200 mg L^{-1}	5 mg L^{-1}	Layer-by-layer assembly method	7	[130]
CdS/P_2MoxW_{18x} nanospheres with type II heterostructure	64	Chromium(VI)	30 mg	40 mg L^{-1}		5–6	[134]
Carbon dot-sensitized urchin-like Ti^{3+} self-doped TiO_2	-	Chromium(VI)	1 g L^{-1}	40 mg L^{-1}	Hydrothermal method	-	[135]
Bismuth-rich $Bi_4O_5BrxI_{2-x}$	88	Chromium(VI)	5 mg	60 mg L^{-1}	-	-	[136]
Bentonite/chitosan/TiO_2 heterostructured catalyst	97	Arsenic(III)	160 mg g^{-1}	15 mg L^{-1}	-	3–10	[137]
WO_3/TiO_2 nanomaterials	99	Arsenic(III)	1 g L^{-1}	0.01–4 mg L^{-1}	Sol gel method	7	[131]
Bi_2WO_6/Na-bentonite composites	-	Arsenic(III)	0.2 g L^{-1}	10 mg L^{-1}	Hydrothermal method	> 7.1	[138]
Nano tin ferrous oxide decorated graphene oxide sheets	-	Arsenic(III)	1 g L^{-1}	10–400 mg L^{-1}	Batch adsorption method	6–8	[139]
Bismuth-based photocatalyst	76	Mercury	-	-	Hydrothermal method	2.03–3.05	[140]

Cr(VI) to Cr(III) [151]. Cr(VI) ions are more mobile and soluble throughout a more excellent pH range, making this the case. Photocatalytic nanoparticles for chemical reduction are one example. The photocatalytic reduction seems an efficient and environmentally benign method for removing Cr(VI) ions from water. Photocatalytic nanoparticles, such as titanium dioxide (TiO_2), tungsten trioxide (WO_3), and zinc oxide (ZnO), undergo a chemical reaction called photoelectrons when exposed to ultraviolet (UV) or visible light. Positive holes, H^+, drive the reduction of Cr(VI) to Cr(III), whereas electrons, e^-, power the oxidation of Cr(VI) to Cr(III) [152].

Researchers developed and synthesized flowerlike Ag/p-Ag_2O/n-$BiVO_4$ plasmonic photocatalyst for photocatalytic BPA (Bisphenol A) oxidation and chromium(VI) reduction under visible light. The enhancing mechanism for the plasmonic photocatalyst was examined, which might be ascribed to facilitated charge transfer, improved visible light absorbance, and reduced electron-hole pair recombination in Ag/p-Ag_2O/n-$BiVO_4$ [153]. Progress regarding the synthesis of various nanocomposites with their effectiveness in reducing chromium(VI) to chromium(III) is discussed in Table 7. Among different nanocomposites, carbon sphere@nano-Fe_3O_4 and C_3N_4/NH_2–UIO-66 showed 100% reduction of chromium(VI) to chromium(III) in 120 min and 20 min, respectively. C_3N_4/NH_2–UIO-66 showed better performance because g-C_3N_4 (CN) and Zr centers were connected by a Zr-N bond, which reduced the carrier migration distance and significantly improved the separation efficacy of photogeneration carriers.

Photocatalytical Oxidation of Arsenic(III) to Arsenic(V)

Numerous people are at risk due to arsenic contamination of water sources [161, 162]. Arsenic pollution of surface and groundwater often originates from arsenic-containing soil and mineral ores, such as arsenopirite (FeAsS), orpiment (As_2S_3), and realgar (As_4S_4) [25]. Arsenic may be introduced into water sources due to human activity such as herbicides and pesticides, phosphate fertilizers, burning fossil fuels, industrial activities, metal melting, and mining. Arsenic is an element that may be found naturally in the environment, and it often coexists with other elements, such as sulfur, iron, and oxygen, in the composition of different minerals and soils. When combined with certain iron minerals, such as goethite, arsenic(V) can produce highly stable hydroxides. Despite the apparent ease with which arsenic may interact with other species, the adsorption of arsenic is contingent on a variety of parameters, the most important of which are pH and temperature. In this way, arsenic may rapidly seep out, which can contaminate both surface water and groundwater. In addition, certain human activities, such as using fertilizers and phytosanitary pesticides in agricultural settings, might result in the release of as into the groundwater [49].

Arsenic is a naturally occurring, widely distributed element in the earth's crust that has garnered attention owing to its toxicity and significance in the development of cancers, particularly bladder cancer and Blackfoot disease [50, 51]. Arsenic in natural waters is most typically found as arsenite (As(III)) or arsenate (As(V), both oxyanions). Trivalent non-ionized arsenite, H_3AsO_3, dominates in reducing environments, such as aquifers with near-neutral pH, whereas As(V) in the form of H_2AsO_4 or $HAsO_4$ dominates in oxidizing and alkaline environments [52]. Arsenate is stable and less poisonous than arsenite [53]. Arsenate may be removed from water using activated alumina, anionic exchange resins, and coagulation with ferric chloride or alum [54]. However, these approaches' effectiveness and consistency may differ. As(III) may be pre-oxidized using chlorine, hydrogen peroxide, sodium permanganate, and ozone. Many substances can oxidase As(III); however, byproducts or residuals might have unforeseen effects [55]. Heterogeneous photocatalysis is used to remove pollutants from water. When the band gap is stimulated in semiconductors, the hydroxyl radical ($HO^\bullet$ radical) is generated, generating electron-hole pairs (e^-H^+) that may reduce and oxidise molecules. TiO_2 converts

Table 7 Various advanced nanocomposites for effective photoreduction of chromium(VI) to chromium(III)

Composites	Pollutants	Irradiation time	Efficiency (%)	Synthetic method	Ref.
Ag/p-Ag_2O/n-$BiVO_4$	Chromium(VI)	100 min	91.9	In situ reductive reaction	[153]
Mn_3O_4@ZnO/Mn_3O_4	Chromium(VI)	70 min	96	Hydrothermal method	[154]
ZnO/Fe_3O_4-Ca-Alg	Chromium(VI)	180 min	84.5	-	[155]
Carbon sphere@nano-Fe_3O_4	Chromium(VI)	120 min	100	Hydrothermal method	[156]
Ag/Ag_3PO_4/rGO microspheres	Chromium(VI)	30 h	90	Electrostatic spraying	[157]
PES/(CHI-ALG)3.5/Fe0@WO_3	Chromium(VI)	-	99.2	Series of reactions	[130]
$BiVO_4$/$FeVO_4$@rGO	Chromium(VI)	90 min	90.9	Hydrothermal method	[158]
C_3N_4/NH_2–UIO-66	Chromium(VI)	20 min	100	Solvothermal method	[159]
$CoFe_2O_4$/ZrO_2	Chromium(VI)	180 min	83	Hydrothermal method	[160]

As(III) to As(V) in the presence of oxygen. This material's strong $e^{-}H^{+}$ pair recombination rate decreases photon efficiency. Researchers have produced novel materials to solve this problem by (i) doping TiO_2 with transition metal ions or nonmetal or (ii) integrating additional semiconductor oxides like CuO, ZrO_2, Fe_2O_3, MnO_2, GaO_2, SnO_2, and WO_3.

The accumulation of arsenic in the body due to its consumption leads to numerous forms of cancer and other serious illnesses, one of which is called arsenicosis. As a result of the bioaccumulative, toxic, and carcinogenic properties of the substance, the WHO lowered the limit for the amount of As that may be present in drinking water from 50 mg L^{-} to 10 g L^{-1} [56]. There is a possibility that the Duero Basin in Spain has arsenic concentrations that are as high as 10 mg L^{-1} [57]. Due to the presence of hazardous levels of arsenic in the drinking water in several Spanish villages in the Duero Basin in recent years, the water supply has been cut off to those areas.

Photocatalytic oxidation processes, which use UV radiation with nanoparticles like Fe_2O_3, TiO_2, and ZnO, have been documented in numerous reports due to their use of mild oxidants and potential to replace conventional high-energy treatment techniques [7, 77]. The oxidation of As(III) by ultraviolet-a (UVA) light in the presence of iron (Fe) compounds and Fe nano-oxides is a necessary photocatalytic process. Research has revealed that manganese (Mn) nano-oxides are as effective as, if not more effective than, iron (Fe) oxides for oxidising arsenite. Since using two or more metals in a single combination has an additive effect on each metal, researchers have recently focused on the bimetal nano-oxides compound to study how it promotes distinct oxidation and adsorption of arsenic from aqueous environments [78]. Over the past few years, much work has been done to reduce arsenic(III) to arsenic (V), which is discussed in Table 8. Among various composites, TiO_2@Fe_3O_4 showed remarkably extraordinary performance and showed a reduction of arsenic to 100% within 4 min. This was due to the unique Ti-O-Fe linkage in the composite, which efficiently promoted the separation of photogenerated carriers and improved its transfer efficiency.

Photocatalytic Oxidation of Mercury(0) to Mercury(II)

Human beings must address three urgent global issues as industry and civilization grow: efficiency in energy usage, energy conversion, and pollution [79, 80]. Today, most of the world's power is produced by nonrenewable energy sources, including coal, petroleum, and natural gas. Chimney gas from coal-fired power plants contains a wide variety of contaminants, and these contaminants' impacts on the environment are becoming increasingly pronounced. In addition, the severity of the principal pollutants–such as SO_x, NO_x, and hazardous particles–and the contaminants that include trace amounts of heavy metals, such as mercury (Hg^0), are worsening [81–83]. Because of its high toxicity, extensive distribution, and bioaccumulative properties, mercury is a global pollutant that risks human and environmental health. Natural ejections and human actions are the two most essential mercury resources [84, 85]. The most frequent biological processes that release mercury into the environment include plant respiration, forest fires, geothermal activity, soil pollution, volcanic eruptions, and evaporation from ocean water [9]. Around 5000 tons of mercury are contaminated yearly, with most of the pollution caused by human activity. Both mercury vapor and mercury salts have the property of hyper toxicity, which makes them potentially harmful to human health if breathed or consumed.

The majority of scientists think that the biggest single human-caused source of distinctive mercury ejections comes from coal-fired power plants (CFPPs). According to research done by the United Nations Environment Program (UNEP) Global Mercury Assessment, coal-fired power plants are thought to discharge 1470 tons of mercury annually around

Table 8 Various advanced nanocomposites for effective photoreduction of arsenic(III) to arsenic(V)

Composite	Pollutant	Irradiation time (min)	Efficiency (%)	Synthetic method	Ref.
$BiVO_4/TiO_2$	Arsenic(III)	90	99.9	Ultrasonic treatment	[163]
γ-Fe_2O_3@PANI@TiO_2	Arsenic(III)	300	92	Photocatalytic oxidation–adsorption process	[164]
TiO_2/PTh/γ-Fe_2O_3	Arsenic(III)	300	99.1	One-pot synthesis	[165]
Fe_2O_3-Mn_2O_3	Arsenic(III)	30	> 99	-	[166]
$ZnFe_2O_4$/Ag/AgCl coupled peroxymonosulfate	Arsenic(III)	20	70.6	Hydrothermal	[167]
C-TiO_2/AC	Arsenic(III)	150	58.4	Sol–gel method	[168]
TiO_2@Fe_3O_4	Arsenic(III)	4	100	Ultrasonic	[169]
WO_3/TiO_2	Arsenic(III)	25	99	Sol–gel method	[131]

the world. Other notable resources of mercury contamination include gold mines (300 tons), cement factories (130 tons), landfills (110 tons), and mercury-producing facilities (200 tons). Since the onset of "Minamata illness" in the late 1950s, industrialization has been linked to an increase in mercury pollution in the USA [86], Finland [26], China, and other Asian nations [59].

Mercury in the flue gas from coal combustion exists in three different states: Hg^0 (the elemental form), Hg^{2+} (from divalent atoms), and Hg^0 (attached to particles) [60, 61]. Most of the mercury is converted to the non-reactive, elemental form in flue gas at temperatures between 700 and 800 °C (Hg^0). As the flue gas passes through the different phases of the heat changer, some of the Hg^0 reacts with the fly ash and other elements to create divalent ion mercury (Hg^{2+}) and particulate mercury (Hg^0). Electrostatic precipitators (ESP), fabric filters (FF), and other devices may capture particulate-bound mercury. Still, divalent mercury can be successfully detached by a wet flue gas desulfurization (WFGD) system since it is water-soluble [62]. Hg^0, which accounts for a significant portion of flue gas, has the characteristics of high volatility. Additionally, it cannot be absorbed, dissolved in water, or broken down by microbes [63]. As a result, mercury removal competence in flue gas from coal-fired control plants is low due to the purification technology now in use in power plants. Hg^0 must be eliminated from power plant flue gas as soon as feasible because of its serious threats to human health and life.

Research into semiconductor photocatalytic equipment like TiO_2 has emerged as a viable area of study in the decades after the 1972 discovery by Fujishima and Honda that semiconductor TiO_2 may electrolyze water to create hydrogen on the electrode. Photocatalytic technology was first employed to treat environmental contaminants in earnest when Carey et al. (1976) used TiO_2 materials to photocatalyst the breakdown of organic biphenyls and chlorinated biphenyls [64]. Since it has the potential to provide both energy and environmental remediation, photocatalytic processes, such as converting solar energy to fuels using a semiconductor photocatalyst, are receiving a great deal of interest [65–67]. Importantly, Hg^0 in its gaseous form may be effectively removed using photocatalytic oxidation technology. Photocatalytic technology has been used to oxidize successfully. A large band gap, which limits the excitation of the pure semiconductor to the UV, a poor electron transfer rate, and a high recombination rate of photogenerated electron-hole pairs are all limitations that limit photocatalytic performance [67]. Because of its large band gap (anatase 3.20 eV, rutile 3.02 eV), conventional TiO_2 must be exposed to UV light to be activated. TiO_2 photocatalyst's poor quantization yield and inadequate oxidation ability severely limit its widespread deployment since the excited electron-hole pairs readily recombine and are difficult to transport to the catalyst's surface for the subsequent reaction. So, it has become a new challenge in photocatalysis research to create novel photocatalysts that can be stimulated by visible light. $BiOIO_3$ photocatalysts irradiated with UV and LED light were used to extract gaseous elemental mercury. The precursor pH determined the $BiOIO_3$ crystal structure and shape. $BiOIO_3$ products only formed under acidic environments. Nearly all Hg^0 was removed from a $BiOIO_3$ nanosheet sample exposed to UV light (25 min) and LED light (100 min). Hg^0 removed the pollutant more effectively than P25 (UV light: 77%; LED light: 42%). Photogenerated holes oxidized Hg^0. Hg^0 oxidation removal might employ newly discovered $BiOIO_3$ photocatalysts, which were both active and stable, as shown in Fig. 6 [27].

Among various composites discussed in Table 9, $BiOIO_3$/g-C_3N_4 and AgI-BiOI/$CoFe_2O_4$ showed the best performance for mercury removal by the photocatalytic process. $BiOIO_3$/g-C_3N_4 showed better performance because of the unique nanoflake heterostructure between them. $BiOIO_3$ was deposited on carbon nitride, which resulted in enhanced charge transfer, facilitating the photocatalytic oxidation of mercury.

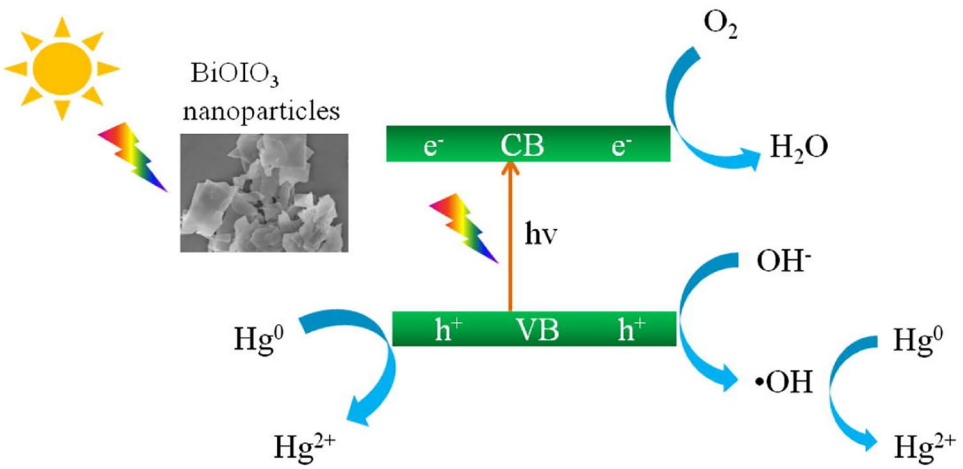

Fig. 6 Mechanism depicting oxidation of mercury by $BiOIO_3$ nanoparticles by photocatalytic mechanism indicating by sun irradiation. Reprinted from Ref. [27] with permission from Elsevier. License Number: 5436000060673

Table 9 Various advanced nanocomposites for effective photo-oxidation of Hg(0) to Hg(II)

Composites	Pollutant	Irradiation time (min)	Efficiency (%)	Synthetic method	Ref.
$BiOIO_3$/g-C_3N_4	Hg^o	120 min	97.3	Improved calcination process	[170]
AgI-BiOI/$CoFe_2O_4$	Hg^o	60 min	97	Solvothermal	[171]
TiO_2/RGO	Hg^o	-	83.7	-	[172]
VO-BWO/CN	Hg^o	60 min	87.2	Ultrasonic treatment	[173]
CeO_2/BiOI	Hg^o	30 min	63.7	Solvothermal	[174]
TiO_2/g-C_3N_4	Hg^o	120 min	70.3	Ultrasonic treatment	[175]
CeO_2/BiOBr/rGO	Hg^o	45 min	76.3	Solvothermal	[176]
MnO_2/TiO_2	Hg^o	45 min	91.2	Hydrothermal method	[177]
I-Bi_2MoO_6	Hg^o	120 min	95.2	Ultrasonic treatment	[178]

Conclusions

The main idea beyond this review article was to highlight recent achievement in the removal of hazardous metal ions from wastewater by nanocomposites/monohybrids through advanced remediation processes and photocatalytic oxidation. The comprehensive summary of this data will give an overview to facilitate the efficient removal of toxic metals. Metals like As, Hg, and Cr are slowly building up in the world's water supply, presenting a hazard to aquatic and human life. Carbon, polymer, and semiconductor nanoparticles offer distinct structural and chemical properties for eliminating As, Hg, and Cr ions from wastewater. Due to their large surface area and porosity, nanomaterials such as graphene oxide, titania, polymeric nanofiber, chitosan, and activated carbon rapidly adsorb As, Hg, and Cr ions from aqueous solutions. Simple approaches may create and modify nanomaterials with improved selectivity, tuneability, and performance. Due to their deeper penetration, these materials can treat water and wastewater in ways not possible with standard approaches. Advanced nanomaterials can photocatalytically oxidize or reduce heavy metals. Using amalgam materials with a mechanical loom, including photocatalytic and adsorption, yields excellent results. This nanotechnological approach may depend on them. The ability of functional nanomaterials to adsorb As, Hg, and Cr ions depends on pH and adjacent intentional groups. Remarkable outcomes are achieved using amalgam materials with a combined mechanical loom incorporating photocatalytic and adsorption processes. They may be the key to the economic success of this nanotechnological strategy. Nanomaterials' potential, current constraints, and regulatory frameworks for water treatment were also examined. This study will help develop new nanomaterials in the near future to effectively remove pollutants. Thorough economic analysis as well as attempts to transfer developed solutions from lab-scale into wider use should be the next step in the production of efficient techniques for the removal of hazardous metal ions from wastewater.

Funding The research leading to these results has received funding from the Norwegian Financial Mechanism 2014-2021 under Project number 2020/37/K/ST8/03805 (MB). This work was supported by the National Science Centre, Poland underthe resear ch Grant number 2019/35/D/ST8/02087 (JZ). CONACyT is thankfully acknowledged for supporting this work under SNI program awarded to Hafiz M.N. Iqbal (CVU: 735340).

Compliance with Ethical Standards

Conflict of Interest The author(s) declare no conflicting interests.

Human and Animal Rights and Informed Consent This article does not contain any studies with human or animal subjects performed by any of the authors.

References

1. Khare J. Heavy metal toxicity in the ecosystem and its impacts. Global J Eng Sci Soc Sci Stud. 2016;2.
2. Tahir MB, Kiran H, Iqbal T. The detoxification of heavy metals from aqueous environment using nano-photocatalysis approach: a review. Environ Sci Pollut Res. 2019;26(11):10515–28.
3. Farhan A, et al. Metal ferrites-based nanocomposites and nanohybrids for photocatalytic water treatment and electrocatalytic water splitting. Chemosphere. 2023;310:136835.
4. Taseidifar M, et al. Removal of heavy metal ions from water using ion flotation. Environ Technol Innov. 2017;8:182–90.
5. Qasem NA, Mohammed RH, Lawal DU. Removal of heavy metal ions from wastewater: a comprehensive and critical review. Npj Clean Water. 2021;4(1):1–15.

6. Byrne C, Subramanian G, Pillai SC. Recent advances in photocatalysis for environmental applications. J Environ Chem Eng. 2018;6(3):3531–55.
7. Singh R, et al. Arsenic contamination consequences and remediation techniques: a review. Ecotoxicol Environ Saf. 2015;112:247–70.
8. Alka S, et al. Arsenic removal technologies and future trends: a mini review. J Clean Prod. 2021;278:123805.
9. Amin S, et al. Mercury methylation and its accumulation in rice and paddy soil in degraded lands: a critical review. Environ Technol Innov. 2021;23:101638.
10. Feng X, et al. Mercury pollution in China: implications on the implementation of the Minamata convention. Environ Sci Process Impact. 2022;24(5):634–48.
11. Sriram G, et al. Recent trends in the application of metal-organic frameworks (MOFs) for the removal of toxic dyes and their removal mechanism-a review. Sustain Mater Technol. 2021;31:e00378.
12. Farhan A, et al. Multifunctional graphene-based nanocomposites and nanohybrids for the abatement of agro-industrial pollutants in aqueous environments–a review. Environ Pollut. 2022;308:119557.
13. Hakizimana JN, et al. Electrocoagulation process in water treatment: a review of electrocoagulation modeling approaches. Desalination. 2017;404:1–21.
14. Bolisetty S, Peydayesh M, Mezzenga R. Sustainable technologies for water purification from heavy metals: review and analysis. Chem Soc Rev. 2019;48(2):463–87.
15. Vepsäläinen M, Sillanpää M. Electrocoagulation in the treatment of industrial waters and wastewaters. In: Advanced water treatment. Elsevier; 2020. p. 1–78.
16. Sardari K, et al. Aluminum electrocoagulation followed by forward osmosis for treating hydraulic fracturing produced waters. Desalination. 2018;428:172–81.
17. Aswathy P, et al. Removal of organics from bilge water by batch electrocoagulation process. Sep Purif Technol. 2016;159:108–15.
18. Ziouvelou A, Tekerlekopoulou AG, Vayenas DV. A hybrid system for groundwater denitrification using electrocoagulation and adsorption. J Environ Manag. 2019;249:109355.
19. Yavuz Y, Ögütveren Ü. Treatment of industrial estate wastewater by the application of electrocoagulation process using iron electrodes. J Environ Manag. 2018;207:151–8.
20. Deveci EÜ, et al. Enhancing treatability of tannery wastewater by integrated process of electrocoagulation and fungal via using RSM in an economic perspective. Process Biochem. 2019;84:124–33.
21. Wu M, et al. Electrocoagulation method for treatment and reuse of sulphide mineral processing wastewater: characterization and kinetics. Sci Total Environ. 2019;696:134063.
22. Bashir MJ, et al. Post treatment of palm oil mill effluent using electro-coagulation-peroxidation (ECP) technique. J Clean Prod. 2019;208:716–27.
23. Gervas C, et al. Functionalized mesoporous organo-silica nanosorbents for removal of chromium (III) ions from tanneries wastewater. J Porous Mater. 2016;23(1):83–93.
24. Ahmed E, et al. Remediation and recycling of chromium from tannery wastewater using combined chemical–biological treatment system. Process Saf Environ Prot. 2016;104:1–10.
25. Önnby L, et al. Improved arsenic (III) adsorption by Al_2O_3 nanoparticles and H_2O_2: evidence of oxidation to arsenic (V) from X-ray absorption spectroscopy. Chemosphere. 2014;113:151–7.
26. Hynninen V, Lodenius M. Mercury pollution near an industrial source in Southwest Finland. Bull Environ Contam Toxicol. 1986;36:294–8.
27. Qi XM, et al. Fabrication of $BiOIO_3$ nanosheets with remarkable photocatalytic oxidation removal for gaseous elemental mercury. Chem Eng J. 2016;285:11–9.
28. Kumar V, et al. Global evaluation of heavy metal content in surface water bodies: a meta-analysis using heavy metal pollution indices and multivariate statistical analyses. Chemosphere. 2019;236:124364.
29. Minas F, Chandravanshi BS, Leta S. Chemical precipitation method for chromium removal and its recovery from tannery wastewater in Ethiopia. Chem Int. 2017;3(4):291–305.
30. Henryk K, Jarosław C, Witold Ż. Peat and coconut fiber as biofilters for chromium adsorption from contaminated wastewaters. Environ Sci Pollut Res. 2016;23(1):527–34.
31. Zhao N, et al. Environmentally persistent free radicals mediated removal of Cr (VI) from highly saline water by corn straw biochars. Biores Technol. 2018;260:294–301.
32. Jobby R, et al. Biosorption and biotransformation of hexavalent chromium [Cr (VI)]: a comprehensive review. Chemosphere. 2018;207:255–66.
33. Bhati A, et al. Sunlight-induced photoreduction of Cr (VI) to Cr (III) in wastewater by nitrogen-phosphorus-doped carbon dots. npj Clean Water. 2019;2(1):1–9.
34. Mishra T, Mahato DK. A comparative study on enhanced arsenic (V) and arsenic (III) removal by iron oxide and manganese oxide pillared clays from ground water. J Environ Chem Eng. 2016;4(1):1224–30.
35. Navarathna CM, et al. Removal of Arsenic (III) from water using magnetite precipitated onto Douglas fir biochar. J Environ Manag. 2019;250:109429.
36. Bullen JC, et al. On the application of photocatalyst-sorbent composite materials for arsenic (III) remediation: insights from kinetic adsorption modelling. J Environ Chem Eng. 2020;8(5):104033.
37. Türkmen D, et al. Development of ion imprinted based magnetic nanoparticles for selective removal of arsenic (III) and arsenic (V) from wastewater. Sep Sci Technol. 2022;57(6):990–9.
38. Hao L, et al. A critical review on arsenic removal from water using iron-based adsorbents. RSC Adv. 2018;8(69):39545–60.
39. Gworek B, et al. Mercury in marine and oceanic waters–a review. Water Air Soil Pollut. 2016;227(10):1–19.
40. Verma RK, Sankhla MS, Kumar R. Mercury contamination in water & its impact on public health. Int J Forensic Sci. 2018;1(2):72–8.
41. Vöröš D, et al. Mercury contamination of stream sediments in the North Bohemian Coal District (Czech Republic): mercury speciation and the role of organic matter. Chemosphere. 2018;211:664–73.
42. Wang L, et al. Remediation of mercury contaminated soil, water, and air: a review of emerging materials and innovative technologies. Environ Int. 2020;134:105281.
43. Slimani T, et al. Large-scale geographic patterns of mercury contamination in Morocco revealed by freshwater turtles. Environ Sci Pollut Res. 2018;25(3):2350–60.
44. Fu C-C, et al. Highly efficient carbon quantum dot suspensions and membranes for sensitive/selective detection and adsorption/recovery of mercury ions from aqueous solutions. J. Taiwan Institute Chem. Eng. 2019;100:127-136.
45. Zhou Q, et al. Total concentrations and sources of heavy metal pollution in global river and lake water bodies from 1972 to 2017. Glob Ecol Conserv. 2020;22:e00925.
46. Marrugo-Negrete J, Pinedo-Hernández J, Díez S. Assessment of heavy metal pollution, spatial distribution and origin in agricultural soils along the Sinú River Basin, Colombia. Environ Res. 2017;154:380–8.
47. Ertani A, et al. Chromium in agricultural soils and crops: a review. Water Air Soil Pollut. 2017;228(5):1–12.
48. Shahid M, et al. A meta-analysis of the distribution, sources and health risks of arsenic-contaminated groundwater in Pakistan. Environ Pollut. 2018;242:307–19.

49. Garcia-Costa AL, et al. UV-assisted catalytic wet peroxide oxidation and adsorption as efficient process for arsenic removal in groundwater. Catal Today. 2021;361:176–82.
50. Fontana KB, et al. Comparision of photocatalysis and photolysis processes for arsenic oxidation in water. Ecotoxicol Environ Saf. 2018;151:127–31.
51. López-Muñoz M, et al. Removal of As (III) from aqueous solutions through simultaneous photocatalytic oxidation and adsorption by TiO_2 and zero-valent iron. Catal Today. 2017;280:149–54.
52. Zhang Q, et al. Sustainable approach for spent V_2O_5–WO_3/TiO_2 catalysts management: selective recovery of heavy metal vanadium and production of value-added WO_3–TiO_2 photocatalysts. ACS Sustain Chem Eng. 2018;6(9):12502–10.
53. Masliy A, Kuznetsov A, Korshin G. The intrinsic mechanism of catalytic oxidation of arsenite by hydroxyl-radicals in the H_3AsO_3–CO_2–/HCO_3−–H_2O system: a quantum-chemical examination. Chemosphere. 2020;238:124466.
54. Ogata F, Ueta E, Kawasaki N. Characteristics of a novel adsorbent Fe–Mg-type hydrotalcite and its adsorption capability of As (III) and Cr (VI) from aqueous solution. J Ind Eng Chem. 2018;59:56–63.
55. Kim D-H, et al. Spontaneous oxidation of arsenite on platinized TiO_2 through activating molecular oxygen under ambient aqueous condition. Appl Catal B. 2020;260:118146.
56. WHO G. Guidelines for drinking-water quality. World Health Organization. 2011;216:303–4.
57. Luque-Espinar JA, et al. Multiscale analysis of the spatial variability of heavy metals and organic matter in soils and groundwater across Spain. J Hydrol. 2018;561:348–71.
58. Economou-Eliopoulos M, Megremi I. Contamination of the soil–groundwater–crop system: environmental risk and opportunities. Minerals. 2021;11(7):775.
59. Gao J, et al. Pollution characteristics of atmospheric particulate mercury near a coal-fired power plant on the southeast coast of China. Atmos Pollut Res. 2016;7(6):1119–27.
60. Zhao S, et al. A review on mercury in coal combustion process: content and occurrence forms in coal, transformation, sampling methods, emission and control technologies. Prog Energy Combust Sci. 2019;73:26–64.
61. Yang W, et al. Mercury removal from flue gas by magnetic iron-copper oxide modified porous char derived from biomass materials. Fuel. 2019;256:115977.
62. Yang W, et al. Gas-phase elemental mercury removal using ammonium chloride impregnated sargassum chars. Environ Technol. 2019;40(15):1923–36.
63. Yang W, et al. Removal of elemental mercury from flue gas using red mud impregnated by KBr and KI reagent. Chem Eng J. 2018;341:483–94.
64. Carey JH, Lawrence J, Tosine HM. Photodechlorination of PCB's in the presence of titanium dioxide in aqueous suspensions. Bull Environ Contam Toxicol. 1976;16(6):697–701.
65. He R, et al. Review on nanoscale Bi-based photocatalysts. Nanoscale Horiz. 2018;3(5):464–504.
66. Tian N, et al. Rational nanostructure design of graphitic carbon nitride for photocatalytic applications. J Mater Chem A. 2019;7(19):11584–612.
67. Chen P, et al. Bi-based photocatalysts for light-driven environmental and energy applications: structural tuning, reaction mechanisms, and challenges. EcoMat. 2020;2(3):e12047.
68. Kobielska PA, et al. Metal–organic frameworks for heavy metal removal from water. Coord Chem Rev. 2018;358:92–107.
69. Drozhzhin S, et al. Influence of the electrode location on discharge combustion in the processes of chromium coatings formation from $Cr_2(SO)_4$ solutions. In: Journal of Physics: Conference Series. IOP Publishing; 2021.
70. Chen F, et al. Assessment of chromium toxicity and potential health implications of agriculturally diversely irrigated food crops in the semi-arid regions of South Asia. Agric Water Manag. 2022;272:107833.
71. Upadhyay S, Sinha A. A study on different bioremediation approaches to hexavalent chromium. In: Pollution control technologies. Springer; 2021. p. 57–74.
72. Missimer TM, et al. Natural background and anthropogenic arsenic enrichment in Florida soils, surface water, and groundwater: a review with a discussion on public health risk. Int J Environ Res Public Health. 2018;15(10):2278.
73. Varol M. Environmental, ecological and health risks of trace metals in sediments of a large reservoir on the Euphrates River (Turkey). Environ Res. 2020;187:109664.
74. Upadhyay MK, et al. A review of arsenic in crops, vegetables, animals and food products. Food Chem. 2019;276:608–18.
75. Mahmud M, et al. Study of mercury concentration in plants in Traditional Buladu Gold Mining. In: IOP Conference Series: Earth and Environmental Science. IOP Publishing; 2019.
76. Basu N, et al. A state-of-the-science review of mercury biomarkers in human populations worldwide between 2000 and 2018. Environ Health Perspect. 2018;126(10):106001.
77. Ganiyu SO, et al. Coupling of membrane filtration and advanced oxidation processes for removal of pharmaceutical residues: a critical review. Sep Purif Technol. 2015;156:891–914.
78. Zhu G, et al. Porous Fe-Mn-O nanocomposites: synthesis and supercapacitor electrode application. Prog Nat Sci Mater Int. 2016;26(3):264–70.
79. Cai B, et al. Environmental concern-based site screening of carbon dioxide geological storage in China. Sci Rep. 2017;7(1):1–16.
80. Li M, et al. Recent advances on photocatalytic fuel cell for environmental applications–the marriage of photocatalysis and fuel cells. Sci Total Environ. 2019;668:966–78.
81. Li Y-K, et al. Recent advances in nanomaterials for analysis of trace heavy metals. Crit Rev Anal Chem. 2021;51(4):353–72.
82. Liu D, Lu C, Wu J. Gaseous mercury capture by copper-activated nanoporous carbon nitride. Energy Fuels. 2018;32(8):8287–95.
83. Cheng H, et al. Enhanced $PbCl_2$ adsorption capacity of modified kaolin in the furnace using a combined method of thermal pre-activation and acid impregnation. Chem Eng J. 2021;414:128672.
84. Beckers F, Rinklebe J. Cycling of mercury in the environment: sources, fate, and human health implications: a review. Crit Rev Environ Sci Technol. 2017;47(9):693–794.
85. Gworek B, et al. Air contamination by mercury, emissions and transformations–a review. Water Air Soil Pollut. 2017;228(4):1–31.
86. Müller SM. Corporate behaviour and ecological disaster: Dow Chemical and the Great Lakes mercury crisis, 1970–1972. Bus Hist. 2018;60(3):399–422.
87. Kim H-T, et al. Evaluation of arsenic, cadmium, lead and mercury contamination in over-the-counter available dry dog foods with different animal ingredients (red meat, poultry, and fish). Front Vet Sci. 2018;5:264.
88. Malek A, Rao GR, Thomas T. Waste-to-wealth approach in water economy: the case of beneficiation of mercury-contaminated water in hydrogen production. Int J Hydrog Energy. 2021;46(52):26677–92.
89. Malik LA, et al. Detection and removal of heavy metal ions: a review. Environ Chem Lett. 2019;17(4):1495–521.
90. Park J-H, et al. Competitive adsorption of heavy metals onto sesame straw biochar in aqueous solutions. Chemosphere. 2016;142:77–83.
91. Bode-Aluko CA, et al. Adsorption of toxic metals on modified polyacrylonitrile nanofibres: a review. Water Air Soil Pollut. 2017;228(1):1–11.
92. Gendy EA, et al. Removal of heavy metals by covalent organic frameworks (COFs): a review on its mechanism and adsorption properties. J Environ Chem Eng. 2021;9(4):105687.

93. Xu J, et al. A review of functionalized carbon nanotubes and graphene for heavy metal adsorption from water: preparation, application, and mechanism. Chemosphere. 2018;195:351–64.
94. Mashile GP, et al. Recyclable magnetic waste tyre activated carbon-chitosan composite as an effective adsorbent rapid and simultaneous removal of methylparaben and propylparaben from aqueous solution and wastewater. J Water Process Eng. 2020;33:101011.
95. Liu CH, Chuang YH, Chen TY, Tian Y, Li H, Wang MK, Zhang W. Mechanism of arsenic adsorption on magnetite nanoparticles from water: thermodynamic and spectroscopic studies. Environ Sci Technol. 2015;49(13):7726–34.
96. Albatrni H, Qiblawey H, El-Naas MH. Comparative study between adsorption and membrane technologies for the removal of mercury. Sep Purif Technol. 2021;257:117833.
97. Wang X, et al. Simultaneous Cr (VI) reduction and Cr (III) removal of bifunctional MOF/Titanate nanotube composites. Environ Pollut. 2019;249:502–11.
98. Tao E, et al. Zirconium dioxide loaded montmorillonite composites as high-efficient adsorbents for the removal of Cr^{3+} ions from tanning wastewater. J Solid State Chem. 2019;277:502–9.
99. Naushad M, et al. Synthesis and characterization of a new starch/SnO_2 nanocomposite for efficient adsorption of toxic Hg^{2+} metal ion. Chem Eng J. 2016;300:306–16.
100. Shafiabadi M, Dashti A, Tayebi H-A. Removal of Hg (II) from aqueous solution using polypyrrole/SBA-15 nanocomposite: experimental and modeling. Synth Met. 2016;212:154–60.
101. Shahzad A, et al. Mercuric ion capturing by recoverable titanium carbide magnetic nanocomposite. J Hazard Mater. 2018;344:811–8.
102. Tauanov Z, Lee J, Inglezakis V. Mercury reduction and chemisorption on the surface of synthetic zeolite silver nanocomposites: equilibrium studies and mechanisms. J Mol Liq. 2020;305:112825.
103. Naushad M, et al. Green and eco-friendly nanocomposite for the removal of toxic Hg (II) metal ion from aqueous environment: adsorption kinetics & isotherm modelling. J Mol Liq. 2019;279:1–8.
104. Sadeghi M, et al. Removal of Arsenic (III) from natural contaminated water using magnetic nanocomposite: kinetics and isotherm studies. J Iran Chem Soc. 2016;13(7):1175–88.
105. Chowdhury T, et al. Removal of arsenic (III) from aqueous solution using metal organic framework-graphene oxide nanocomposite. Nanomaterials. 2018;8(12):1062.
106. Wu K, et al. Magnetic Fe_3O_4@CuO nanocomposite assembled on graphene oxide sheets for the enhanced removal of arsenic (III/V) from water. Appl Surf Sci. 2019;466:746–56.
107. Song X, et al. Halloysite nanotubes stabilized polyurethane foam carbon coupled with iron oxide for high-efficient and fast treatment of arsenic (III/V) wastewater. Chem Eng Res Des. 2021;165:298–307.
108. Wang Y, et al. Enhanced arsenic removal from aqueous solution by Fe/Mn-C layered double hydroxide composite. Adsorp Sci Technol. 2021;2021:8891643.
109. Veerakumar P, Lin K-C. An overview of palladium supported on carbon-based materials: synthesis, characterization, and its catalytic activity for reduction of hexavalent chromium. Chemosphere. 2020;253:126750.
110. Sharma M, et al. ZnO tetrapods and activated carbon based hybrid composite: adsorbents for enhanced decontamination of hexavalent chromium from aqueous solution. Chem Eng J. 2019;358:540–51.
111. Ibrahim H, et al. Outlook on the carbon-based materials for heavy metal removal. Biointerface Res Appl Chem. 2022;12(4):5303–23.
112. Venkateswarlu S, Lee D, Yoon M. Bioinspired 2D-carbon flakes and Fe_3O_4 nanoparticles composite for arsenite removal. ACS Appl Mater Interfaces. 2016;8(36):23876–85.
113. Islam A, et al. Novel micro-structured carbon-based adsorbents for notorious arsenic removal from wastewater. Chemosphere. 2021;272:129653.
114. Dhoble RM, et al. Removal of arsenic (III) from water by magnetic binary oxide particles (MBOP): experimental studies on fixed bed column. J Hazard Mater. 2017;322:469–78.
115. Tan G, et al. Sorption of mercury (II) and atrazine by biochar, modified biochars and biochar based activated carbon in aqueous solution. Biores Technol. 2016;211:727–35.
116. Xu D, et al. Sulfur rich microporous polymer enables rapid and efficient removal of mercury (II) from water. Chemosphere. 2018;196:174–81.
117. Sellami F, et al. Polymer inclusion membranes based on CTA/PBAT blend containing Aliquat 336 as extractant for removal of Cr (VI): efficiency, stability and selectivity. React Funct Polym. 2019;139:120–32.
118. Kaya A, et al. Removal of Cr (VI) through calixarene based polymer inclusion membrane from chrome plating bath water. Chem Eng J. 2016;283:141–9.
119. Khare P, et al. Microchannel-embedded metal–carbon–polymer nanocomposite as a novel support for chitosan for efficient removal of hexavalent chromium from water under dynamic conditions. Chem Eng J. 2016;293:44–54.
120. Lofrano G, et al. Polymer functionalized nanocomposites for metals removal from water and wastewater: an overview. Water Res. 2016;92:22–37.
121. Sargın İ, Arslan G, Kaya M. Efficiency of chitosan–algal biomass composite microbeads at heavy metal removal. React Funct Polym. 2016;98:38–47.
122. Parlayıcı Ş, Avcı A, Pehlivan E. Electrospinning of polymeric nanofiber (nylon 6, 6/graphene oxide) for removal of Cr (VI): synthesis and adsorption studies. J Anal Sci Technol. 2019;10(1):1–13.
123. Mustafai FA, et al. Microwave-assisted synthesis of imprinted polymer for selective removal of arsenic from drinking water by applying Taguchi statistical method. Eur Polym J. 2018;109:133–42.
124. Liu B, et al. Effective and simultaneous removal of organic/inorganic arsenic using polymer-based hydrated iron oxide adsorbent: capacity evaluation and mechanism. Sci Total Environ. 2020;742:140508.
125. Song Y, Gotoh T, Nakai S. Synthesis of oxidant functionalised cationic polymer hydrogel for enhanced removal of arsenic (III). Gels. 2021;7(4):197.
126. Kong L, et al. One-step construction of hierarchical porous channels on electrospun MOF/polymer/graphene oxide composite nanofibers for effective arsenate removal from water. Chem Eng J. 2022;435:134830.
127. Shan H, et al. Triazine-based N-rich porous covalent organic polymer for the effective detection and removal of Hg (II) from an aqueous solution. Chem Eng J. 2021;426:130757.
128. Hajri AK, et al. Designing of modified ion-imprinted chitosan particles for selective removal of mercury (II) ions. Carbohyd Polym. 2022;286:119207.
129. Albakri MA, et al. Synthesis of a new thiophenol-thiophene polymer for the removal of mercury from wastewater and liquid hydrocarbons. J Colloid Interface Sci. 2021;582:428–38.
130. Kazemi M, Jahanshahi M, Peyravi M. Chitosan-sodium alginate multilayer membrane developed by Fe0@WO_3 nanoparticles: photocatalytic removal of hexavalent chromium. Carbohyd Polym. 2018;198:164–74.
131. Navarrete-Magaña M, et al. Improved photocatalytic oxidation of arsenic (III) with WO_3/TiO_2 nanomaterials synthesized by the sol-gel method. J Environ Manag. 2021;282:111602.
132. Wojtyła S, Baran T. Insight on doped ZnS and its activity towards photocatalytic removing of Cr (VI) from wastewater in the presence of organic pollutants. Mater Chem Phys. 2018;212:103–12.

133. Wang P, et al. A cathodic photoelectrochemical sensor for chromium (VI) based on the use of PbS quantum dot semiconductors on an ITO electrode. Microchim Acta. 2018;185(7):1–7.
134. Liu C, et al. Fabrication of CdS/P2MoxW18-x nanospheres with type II heterostructure for photocatalytic reduction of hexavalent chromium. Mater Sci Semicond Process. 2020;120:105276.
135. Shi C, et al. Carbon dot-sensitized urchin-like Ti^{3+} self-doped TiO_2 photocatalysts with enhanced photoredox ability for highly efficient removal of Cr^{6+} and RhB. J Mater Chem C. 2020;8(7):2238–47.
136. Bai Y, et al. Synthesis of hierarchical bismuth-rich $Bi_4O_5BrxI_2$-x solid solutions for enhanced photocatalytic activities of CO_2 conversion and Cr (VI) reduction under visible light. Appl Catal B. 2017;203:633–40.
137. Saleh S, et al. Photooxidation/adsorption of arsenic (III) in aqueous solution over bentonite/chitosan/TiO_2 heterostructured catalyst. Chemosphere. 2021;280:130583.
138. Yang Q, et al. Synthesis of Bi_2WO_6/Na-bentonite composites for photocatalytic oxidation of arsenic (iii) under simulated sunlight. RSC Adv. 2019;9(51):29689–98.
139. Sharma M, et al. Nano tin ferrous oxide decorated graphene oxide sheets for efficient arsenic (III) removal. Nano-Struct Nano-Objects. 2018;13:82–92.
140. Guan Y, et al. Bismuth-based photocatalyst for photocatalytic oxidation of flue gas mercury removal: a review. J Hazard Mater. 2021;418:126280.
141. Chen F, et al. Efficient construction of bismuth vanadate-based Z-scheme photocatalyst for simultaneous Cr (VI) reduction and ciprofloxacin oxidation under visible light: kinetics, degradation pathways and mechanism. Chem Eng J. 2018;348:157–70.
142. Jing F, et al. MIL-68 (Fe) as an efficient visible-light-driven photocatalyst for the treatment of a simulated waste-water contain Cr (VI) and Malachite Green. Appl Catal B. 2017;206:9–15.
143. Jeong I, et al. A tailored TiO2 electron selective layer for high-performance flexible perovskite solar cells via low temperature UV process. Nano Energy. 2016;28:380–9.
144. Zhang G, et al. Visible light-sensitized S, N and C co-doped polymorphic TiO_2 for photocatalytic destruction of microcystin-LR. Appl Catal B. 2014;144:614–21.
145. Joo J, et al. Enhanced photocatalytic activity of highly crystallized and ordered mesoporous titanium oxide measured by silicon resonators. Anal Chem. 2010;82(7):3032–7.
146. Belver C, et al. Solar photocatalytic purification of water with Ce-doped TiO_2/clay heterostructures. Catal Today. 2016;266:36–45.
147. Fan G, et al. Removal of Cr (VI) from aqueous solutions by titanate nanomaterials synthesized via hydrothermal method. Can J Chem Eng. 2017;95(4):717–23.
148. Cieślak-Golonka M. Toxic and mutagenic effects of chromium (VI). A review. Polyhedron. 1996;15(21):3667–89.
149. Li Y, et al. Removal of Cr (VI) by 3D TiO_2-graphene hydrogel via adsorption enriched with photocatalytic reduction. Appl Catal B. 2016;199:412–23.
150. Wang X, et al. Removal of chromium (VI) by a self-regenerating and metal free g-C_3N_4/graphene hydrogel system via the synergy of adsorption and photo-catalysis under visible light. Appl Catal B. 2017;219:53–62.
151. Liu J, et al. An ecological new approach for treating Cr (VI)-containing industrial wastewater: photochemical reduction. Water Res. 2016;93:187–94.
152. Kazemi M, Jahanshahi M, Peyravi M. Hexavalent chromium removal by multilayer membrane assisted by photocatalytic couple nanoparticle from both permeate and retentate. J Hazard Mater. 2018;344:12–22.
153. Zhao W, et al. Study the photocatalytic mechanism of the novel Ag/p-Ag_2O/n-$BiVO_4$ plasmonic photocatalyst for the simultaneous removal of BPA and chromium (VI). Chem Eng J. 2019;361:1352–62.
154. Li N, et al. Efficient removal of chromium from water by Mn_3O_4@ ZnO/Mn_3O_4 composite under simulated sunlight irradiation: synergy of photocatalytic reduction and adsorption. Appl Catal B. 2017;214:126–36.
155. Bilici Z, et al. Photocatalytic effect of zinc oxide and magnetite entrapped calcium alginate beads for azo dye and hexavalent chromium removal from solutions. J Water Process Eng. 2019;31:100826.
156. Liu F, et al. Simultaneous photocatalytic redox removal of chromium (vi) and arsenic (iii) by hydrothermal carbon-sphere@ nano-Fe_3O_4. Environ Sci Nano. 2019;6(3):937–47.
157. Liu Y, et al. Continuous photocatalytic removal of chromium (VI) with structurally stable and porous Ag/Ag_3PO_4/reduced graphene oxide microspheres. Chem Eng J. 2020;379:122200.
158. Yang R, et al. One-step preparation (3D/2D/2D) $BiVO_4$/$FeVO_4$@ rGO heterojunction composite photocatalyst for the removal of tetracycline and hexavalent chromium ions in water. Chem Eng J. 2020;390:124522.
159. Xu Z, et al. Engineering a rapid charge transfer pathway for enhanced photocatalytic removal efficiency of hexavalent chromium over C_3N_4/NH_2–UIO-66 compounds. Solar RRL. 2021;5(2):2000416.
160. Emadian SS, Ghorbani M, Bakeri G. Magnetically separable $CoFe_2O_4$/ZrO_2 nanocomposite for the photocatalytic reduction of hexavalent chromium under visible light irradiation. Synth Met. 2020;267:116470.
161. Khosravi R, et al. Use of geographic information system and water quality index to assess groundwater quality for drinking purpose in Birjand City, Iran. Desalin Water Treat. 2017;67(1):74–83.
162. Zhang D, et al. In-situ mobilization and transformation of iron oxides-adsorbed arsenate in natural groundwater. J Hazard Mater. 2017;321:228–37.
163. Rahimi B, Ebrahimi A. Photocatalytic process for total arsenic removal using an innovative $BiVO_4$/TiO_2/LED system from aqueous solution: optimization by response surface methodology (RSM). J Taiwan Inst Chem Eng. 2019;101:64–79.
164. Wang Y, et al. A magnetic γ-Fe_2O_3@ PANI@ TiO_2 core–shell nanocomposite for arsenic removal via a coupled visible-light-induced photocatalytic oxidation–adsorption process. Nanoscale Adv. 2020;2(5):2018–24.
165. Liu X, et al. One-pot synthesis of a magnetic TiO_2/PTh/γ-Fe_2O_3 heterojunction nanocomposite for removing trace arsenite via simultaneous photocatalytic oxidation and adsorption. Ind Eng Chem Res. 2020;60(1):528–40.
166. Eslami H, et al. Efficient photocatalytic oxidation of arsenite from contaminated water by Fe_2O_3-Mn_2O_3 nanocomposite under UVA radiation and process optimization with experimental design. Chemosphere. 2018;207:303–12.
167. Lei D, et al. Effective photocatalytic removal of As (III) by $ZnFe_2O_4$/Ag/AgCl coupled peroxymonosulfate: Z-Scheme charge transfer and dual active sites. Appl Surf Sci. 2021;567:150860.
168. Alfarawati RK, et al. Solar photocatalytic removal of arsenic from polluted water using carbon-modified titanium oxide nanoparticles supported on activated carbon. Environ Chem. 2020;17(8):568–78.
169. Xiao M, et al. Enhanced photocatalytic oxidation of As (III) by TiO_2 modified with Fe_3O_4 through Ti-O-Fe interface bonds. Colloids Surf A. 2022;651:129678.
170. Wu J, et al. Constructing interfacial contact for enhanced photocatalytic activity through $BiOIO_3$/g-C_3N_4 nanoflake heterostructure. Catal Commun. 2018;109:55–9.
171. Zhang L-X, et al. Effects of experimental parameters on Hg0 removal over magnetic AgI-BiOI/$CoFe_2O_4$ photocatalysts using wet process. J Fuel Chem Technol. 2018;46(3):365–74.

172. Guan Y, et al. Enhanced photocatalytic activity of TiO_2/graphene by tailoring oxidation degrees of graphene oxide for gaseous mercury removal. Korean J Chem Eng. 2019;36(1):115–25.
173. Zhang Y, et al. Fabrication of Z-scheme VO-Bi_2WO_6/g-C_3N_4 heterojunction composite with visible-light-driven photocatalytic performance for elemental mercury removal. Chem Eng J. 2021;425:131537.
174. Xiao Y, et al. Construction of CeO_2/BiOI S-scheme heterojunction for photocatalytic removal of elemental mercury. Appl Surf Sci. 2021;556:149767.
175. Tang T, et al. Tuning dimensionality TiO_2/g-C_3N_4 heterostructure for enhanced elemental mercury removal performance under visible-light. Chem Phys Lett. 2021;782:139027.
176. Jia T, et al. Self-grown oxygen vacancies-rich CeO_2/BiOBr Z-scheme heterojunction decorated with rGO as charge transfer channel for enhanced photocatalytic oxidation of elemental mercury. J Colloid Interface Sci. 2021;587:402–16.
177. Xie C, et al. Evaluation of visible photocatalytic performance of microwave hydrothermal synthesis of MnO_2/TiO_2 core-shell structures and gaseous mercury removal. Microporous Mesoporous Mater. 2022;334:111788.
178. Zhang Y, et al. Enhanced photocatalytic Hg0 oxidation activity of iodine doped bismuth molybdate (Bi_2MoO_6) under visible light. J Colloid Interface Sci. 2022;607:1864–75.